Brain Structure and Function (2022) 227:2127–2151
https://doi.org/10.1007/s00429-022-02507-9

ORIGINAL ARTICLE

GABAergic interneurons' feedback inhibition of dorsal raphe-projecting pyramidal neurons of the medial prefrontal cortex suppresses feeding of adolescent female mice undergoing activity-based anorexia

Muzi Du[1,2] · Adrienne Santiago[1,3] · Cenk Akiz[1] · Chiye Aoki[1,4]

Received: 27 September 2021 / Accepted: 30 April 2022 / Published online: 30 May 2022

Abstract

Anorexia Nervosa (AN) is characterized by voluntary food restriction, excessive exercise and extreme body weight loss. AN is particularly prevalent among adolescent females experiencing stress-induced anxiety. We used the animal model, activity-based anorexia (ABA), which captures these characteristics of AN, to reveal the neurobiology underlying individual differences in AN vulnerability. Dorsal raphe (DR) regulates feeding and is recruited when coping inescapable stress. Through chemogenetic activation, we investigated the role of mPFC pyramidal neurons projecting to DR (mPFC→DR) in adolescent female mice's decision to eat or exercise following ABA induction. Although the DREADD ligand C21 could activate 44% of the mPFC→DR neurons, this did not generate significant group mean difference in the amount of food intake, compared to control ABA mice without chemogenetic activation. However, analysis of *individual*s' responses to C21 revealed a significant, positive correlation between food intake and mPFC→DR neurons that co-express cFos, a marker for neuronal activity. cFos expression by GABAergic interneurons (GABA-IN) in mPFC was significantly greater than that for the control ABA mice, indicating recruitment of GABA-IN by mPFC→DR neurons. Electron microscopic immunohistochemistry revealed that GABAergic innervation is 60% greater for the PFC→DR neurons than adjacent Layer 5 pyramidal neurons without projections to DR. Moreover, individual differences in this innervation correlated negatively with food intake specifically on the day of C21 administration. We propose that C21 activates two antagonistic pathways: (1) PFC→DR pyramidal neurons that promote food intake; and (2) GABA-IN in the mPFC that dampen food intake through feedback inhibition of mPFC→DR neurons.

Keywords Anorexia nervosa · Serotonin · Food restriction · Stress-induced anxiety · Feedback inhibition

Introduction

Anorexia Nervosa (AN) is an eating disorder that affects approximately 2.1 million people world-wide (Global Burden of Disease Study 2013 Collaborators 2013). The characteristic symptoms of AN include voluntary food restriction in pursuit of thinness, compulsive and over-valued thoughts on body shape and weight, as well as failure to maintain a healthy body weight (Attia 2010). AN is highly comorbid with anxiety and mood disorders (Hudson et al. 2007; Merikangas et al. 2010), and has a mortality rate of around 10%. AN is still without approved pharmacological treatment, making AN one of the deadliest among mental illnesses (Arcelus et al. 2011; Birmingham et al. 2005).

Muzi Du and Adrienne Santiago are shared first authors.

✉ Chiye Aoki
ca3@nyu.edu

1 Center for Neural Science, New York University, New York, NY 10003, USA

2 The Solomon H. Snyder Department of Neuroscience, Johns Hopkins University, School of Medicine, Baltimore, MD 21205, USA

3 New York State Psychiatric Institute, Columbia University Irving Medical Center, New York, NY 10032, USA

4 Neuroscience Institute, NYU Langone Medical Center, New York, NY 10016, USA

The neurobiological mechanisms and the treatment for AN remain unresolved.

A rodent model called Activity-Based Anorexia (ABA) captures several key symptoms of AN. Upon giving mice free access to running wheels prior to a few days with restricted food access, some but not all animals undergo voluntary hypophagia and increased wheel running (Hall et al. 1953). These behaviors are maladaptive, since hyperactivity does not improve food access, but instead causes heightened energy expenditure that could be lethal. The major difference between ABA and AN is that, in the ABA model, food restriction (FR) is initially imposed by experimenters. However, this phase is followed by voluntary FR, one hallmark of AN, in that animals choose to run rather than eat, even during the limited hours of food availability. In sum, ABA captures the following essential elements of AN: severe weight loss, extensive exercise even during the limited hours of food availability, and anxiety. The significance of this model lies in its potential to shed light on the neurobiological underpinnings of anorexia-like behaviors in rodents (Chowdhury et al. 2019; Chowdhury et al. 2013; Foldi et al. 2017; Santiago et al. 2021), through which the mechanism of as well as the treatments for patients with AN can be enlightened.

Individuals are the most susceptible to AN during adolescence (Kaye et al. 2009). This period is marked by significant changes in metabolism, endocrine system and brain development, but also by individuals' psychological and socio-cultural transitions (Connan et al. 2003; Fuhrmann et al. 2015; Giedd et al. 1999). Those transitions, whether physiological or mental, could be stressful for individuals. As a result, despite an increased resilience to physical diseases and injuries, the mortality rate during adolescence doubles rather than decreases (Dahl 2004). Therefore, the intense stress faced during this adolescent transition might contribute to the development of eating disorders such as AN. Indeed, individuals diagnosed with AN commonly report the experience of mental stress (Ball and Lee 2000), and AN-like behaviors could be induced by chronic stress in rats (Marti et al. 1994). Therefore, the ability to handle stress effectively may be essential for protecting individuals from developing AN.

The neural circuits underlying stress response may be a neurobiological target for AN pathology. The dorsal raphe nucleus (DR) is an integral component of the serotonin (5-HT) system in the central nervous system. The DR responds potently to external stress, such as motion restraints and early maternal separation (Grahn et al. 1999; Hardaway et al. 2015; Nichols et al. 2017; Pollano et al. 2018). Furthermore, a recent study using optogenetic tools revealed a causal relationship between activation of the serotonergic neurons in DR and active coping under inescapable stress in rats and mice (Nishitani et al. 2019). Anatomically, GABAergic interneurons (GABA-IN) in DR receive inputs from Layer 5 pyramidal neurons in the medial prefrontal cortex (mPFC) (Jankowski and Sesack 2004). mPFC is implicated in various higher-order cognitive functions such as learning, memory and decision-making and we have previously implicated this brain region in ABA running (Santiago et al. 2021). Activation of mPFC projections to DR (mPFC→DR neurons) induces active coping within adverse environments and challenges, such as the forced swim test (Warden et al. 2012). mPFC→DR neurons also engage the controllability of escapable foot-shock stress, which leads to the blockade of the DR-induced behavioral outcomes in face of inescapable stress (Amat et al. 2005). Those results imply that mPFC→DR neurons may mediate higher-order control of mental and starvation stress in AN to initiate either active or passive coping strategies such as extensive exercise versus feeding.

Beside its involvement in stress responses, another well-studied role of DR is to regulate feeding behaviors (Bendotti et al. 1986; Fletcher and Davies 1990). DR neurons have differential activities at different phases of feeding, and are significantly more active during ingestion than food searching and satiety (Takase and Nogueira 2008). Similarly, while feeding increases the activity of the serotonergic neurons in DR, fasting has the opposite effects of reducing their activities (Nectow et al. 2017). Optogenetic activation of the serotonergic neurons in DR suppresses feeding, while activation of GABAergic interneurons in the same area increases feeding (Nectow et al., 2017). Furthermore, at the molecular level, deletion studies show that the 5-HT_4 receptors in the mPFC-DR pathway are required for the development of stress-induced hypophagia (Compan et al. 2015; Jean et al. 2017). Interestingly, even though feeding involves various sensory modalities such as vision and smell, DR as a feeding regulator actually does not receive any direct input from the primary sensory or motor cortices (Weissbourd et al. 2014). This raises the possibility that the regulation of feeding by DR may involve higher-order controls, such as the voluntary decision-making to restrict food intake seen in individuals diagnosed with AN.

Given the multiple cognitive functions of mPFC, we sought to determine whether mPFC→DR neurons may affect feeding in the ABA model, in which animals that exhibit anorexia-like behaviors make the decision to run or to eat. We report on the feeding behaviors of mice during the ABA schedule in response to the excitation or inhibition of mPFC→DR pathway. We show strong correlations between the activities of the mPFC→DR pyramidal neurons in mPFC and food intake of mice. We further reveal the local microcircuits in mPFC that strongly modulate the mPFC→DR pathway and feeding of ABA mice.

Materials and methods

Animals

Eighteen female mice (wild type C57BL6/J, bred at NYU) were used in this study. Starting from postnatal day 26 ± 2 days (P26 ± 2), all animals were singly housed at NYU animal facility under a 12:12 light/dark cycle with the light starting at 7 AM and ending at 7 PM. Water and food were provided ad libitum unless specified. All of the animal handlings adhered to NYU protocols approved by the Institutional Animal Care and Use Committees of New York University (A3317-01).

Surgery for transfection of the mPFC with multiplexed-retro DREADD

In this study, multiplex Designer Receptors Exclusively Activated by Designer Drugs (DREADDs) were used to target the group of neurons projecting from mPFC to DR (mPFC→DR neurons). This chemogenetic approach resembled the methods described in another recent publication from this lab, except that the Multiplexed-Retro DREADD induction targeted the mPFC→DR neurons, rather than the mPFC-to-dorsal striatum pyramidal neurons (Santiago et al. 2021). At P26 ± 2, animals were anesthetized with isoflurane for surgery. For the DREADD experimental animals ($N = 7$, randomly selected among P26 ± 2 mice available at the time of surgery, to be referred to as the DREADD group), viruses containing exogenous genes were transcranially injected through Nanoject II Auto-Nanoliter Injector (#3-000-204, Drummond) at different sites: DR was injected with a retrogradely transported AAV carrying a Cre-EBFP construct (AAVrg-EBFP-Cre) (Han et al. 2018; Tervo et al. 2016). The volume was 400–500 nL, comprised of AAV-rg-pmSyn1-EBFP-Cre (gift from Hongkui Zeng; Addgene viral prep # 51,507-AAVrg; RRID: Addgene_51507; viral titer of 6×10^{12} vg/mL). The stereotaxic coordinates for DR were AP = 0 from Lambda, ML + 0.8 mm @15°, DV 3.3 mm (Correia et al. 2017). The same animals received viruses encoding Cre-dependent hM3D(Gq)-mCherry DREADDs (Gq-DREADDs) (AAV8-hSYN-DIO-hM3D(Gq)-mCherry, gift from Bryan Roth, viral prep # 44361-AAV8; RRID: Addgene_44361; viral titer of 4×10^{12} vg/mL) and Cre-dependent KORD-mCitrine DREADDs (KORD) (AAV1-hSYN1-dF-HA-KORD.IRES.mCitrine, a generous gift from Dr Shaham, Yavin of NIDA, produced by the Genetic Engineering and Viral Vector Core of NIDA; viral titer of 2×10^{12} vg/mL) simultaneously into mPFC using the stereotaxic coordinates of AP 1.8 mm from Bregma, ML ± 0.32 mm, DV 1.5 mm as a 50:50 mixture, 100 nl per hemisphere.

Control animals were injected viruses encoding the CaMKIIα-dependent eGFP (gift from Bryan Roth; Addgene viral prep #50469-AAV8; RRID: Addgene_50469, 1×10^{13} vg/mL), to express GFP in CaMKIIα + pyramidal cells in mPFC without co-expression of DREADD. Alternatively, control animals received the virus encoding Cre-dependent DREADDs but without the retrograde-Cre viruses in DR. The two control subgroups were pooled after verifying through statistical tests that they lacked behavioral differences and will be referred to as the CON group.

ABA schedule

The schematic illustrations for the ABA schedule are included in Fig. 1a for the first ABA induction (ABA1) and for the second ABA induction (ABA2, Fig. 2a).

After ten days of recovery from surgery, at P36 ± 2, an acclimation phase began, whereby animals had 24 h/day access to a running wheel (Low-Profile Wireless Running Wheel for Mouse ENV-044, Med Associates, Fairfax, VA; 2654.86 wheel turn counts per km run) in addition to ad libitum food and water (Pre1, Pre2, Pre3, Pre4, Pre5). The food was of two types: dry food pellet (LabDiet Rodent Diet 20 EXT 5033, 4.5% crude fat, 20% protein, 6% crude fiber, 7% ash, 12% maximum moisture with 4.07 gross energy kca/g, equal to 3.07 metabolizable energy kcal/g) and wet food (Clear H_2O brand DietGel 76A in plastic cups, 0.998 kcal/g, 4.7% protein, 17.9% carbohydrates, 1.5% fat, 73.4% moisture). Following 5 days of wheel acclimation (P41 ± 2), the food was removed at 1 PM, leaving the animal only with free access to the running wheel (first ABA induction, ABA1), an empty food hopper and water gels (Clear H_20 brand Hydrogels Product #70-01-5022, 0 kcal/g). In the following three days, food access was given only between 7 and 9 PM and the animals' food intake during the two-hours of food availability were measured. At noon of the third day of food restriction (FR) (P44 ± 2), ad libitum food access was restored and the running wheel was removed from the cage. After six days of recovery from ABA1 (P50 ± 2), the running wheel was reintroduced to the cage for four days followed by a second ABA induction (ABA2) comprised of four days of food restriction (FR) between 1 PM of FR1 (P54 ± 2) and 1 PM of FR4 (P58 ± 2).

ABA2 was the same as ABA1, with the following exceptions: on FR2, Gq-DREADD's ligand Compound 21 (C21; Tocris, Cat. No. 5548, 1 mg/kg body weight, suspended in sterile saline from a stock solution dissolved in DMSO) was injected intraperitoneally at 3:30 PM and 9:30 PM; on FR4, KORD-DREADD's ligand salvinorin B (SalB; Cayman Chemical, Cat. No. 23582, 10 mg/kg body weight, dissolved in DMSO, then suspended 1:5 in sunflower oil)

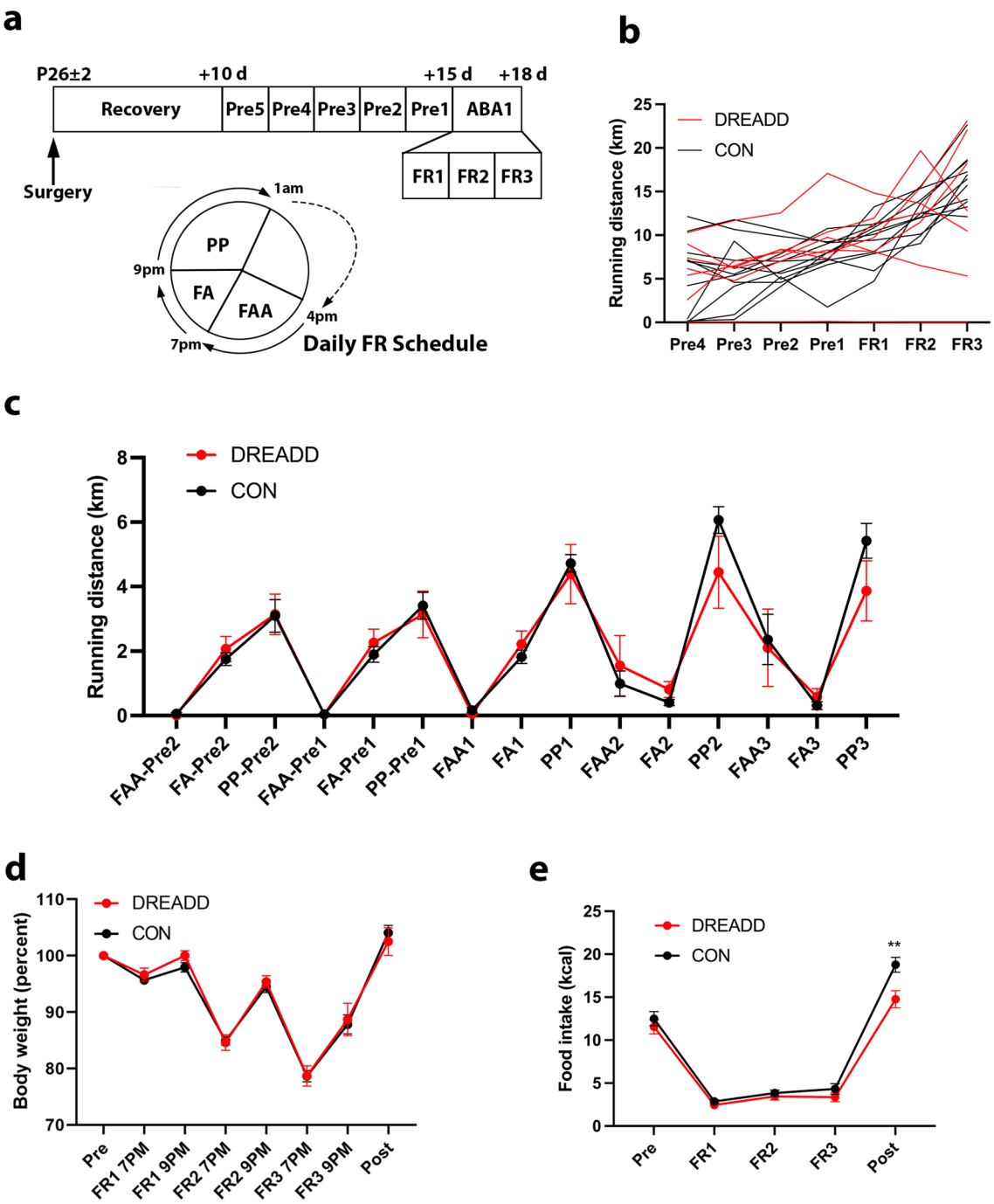

Fig. 1 ABA1 timeline and behavior. **a** Schematic illustration of the first ABA induction and the daily food restriction (FR) schedule. See "Method" section for the details of the ABA1 induction. FAA: food anticipatory activity; FA: food availability; PP: post prandial period. **b** Individual daily wheel running, calculated based on the conversion of 2654.86 wheel turn counts per km; **c** Wheel running during ABA; **d** Body weight; **e** Food intake during the pre-ABA and the three days of FR. The average daily food intake during the two days before the onset of FR on P41 was used as the Pre-ABA baseline food intake. The average daily food intake during the two days after ABA, on P44, was used as the post-ABA food intake. Values in panels (**c–e**) are shown as mean ± SEM. $^{**}p < 0.01$ in panel (**e**)

was injected subcutaneously at 3:30 PM and 6:30 PM. The time points of the two DREADD ligands were chosen to be the same as the time points used for the previous study (Santiago et al. 2021), in which we analyzed the impact of chemogenetic modulation of the PFC-to-dorsal striatum pathway upon FR-evoked hyperactivity and food consumption. This was so that we could maximize our comparison of the two pathways' regulation of ABA behavior. The two

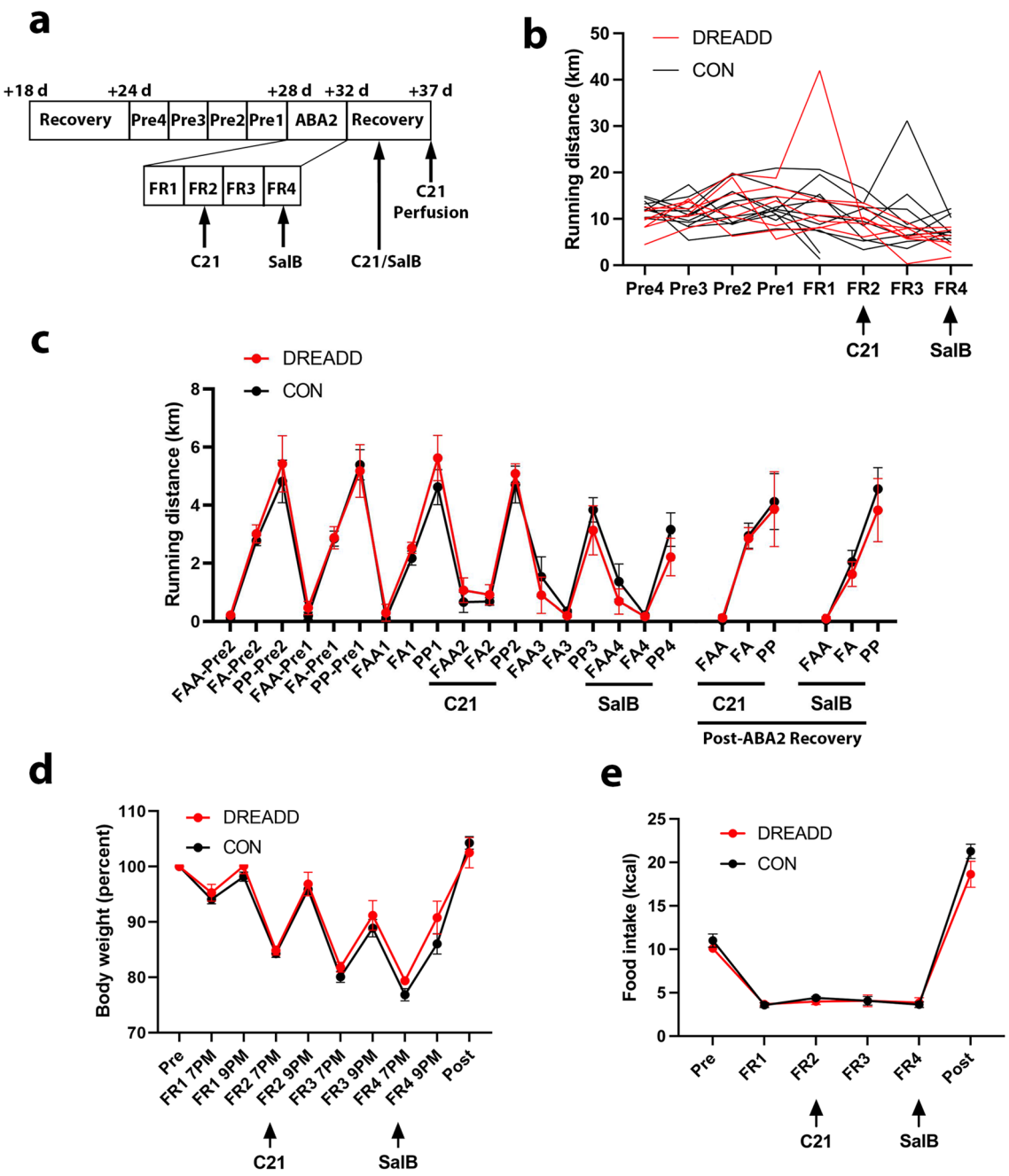

Fig. 2 ABA2 timeline and behavior. **a** Schematic illustration of the second ABA induction. See "Method" section for the details of the second ABA induction. **b** Wheel running of individual animals. **c** Wheel running of DREADD and CON groups. **d** Body weight; **e** Food intake during the pre-ABA and the four days of food restriction. * indicates $p \leq 0.05$. Values in panels (**c–e**) are shown as mean ± SEM

injections of C21 were spaced farther apart than the two injections of SalB, based on the report that C21 drug activity lasts longer than that of SalB (Chen et al. 2015; Thompson et al. 2018; Vardy et al. 2015).

The procedures for drug suspension and systemic injections also followed the protocols described earlier by the same authors. Starting from 1 PM at the end of FR4, the animals went through 4–7 days of recovery, whereby they had ad libitum access to food and wheel. During one of the days of recovery, C21 was injected, while on another of the days of recovery, SalB was injected, for assessing whether the DREADD ligands' effects on behavior depended on FR. Lastly, C21 was administered ~90 min before euthanasia for all DREADD mice, to assess DREADD-induced activity in various mPFC cell populations.

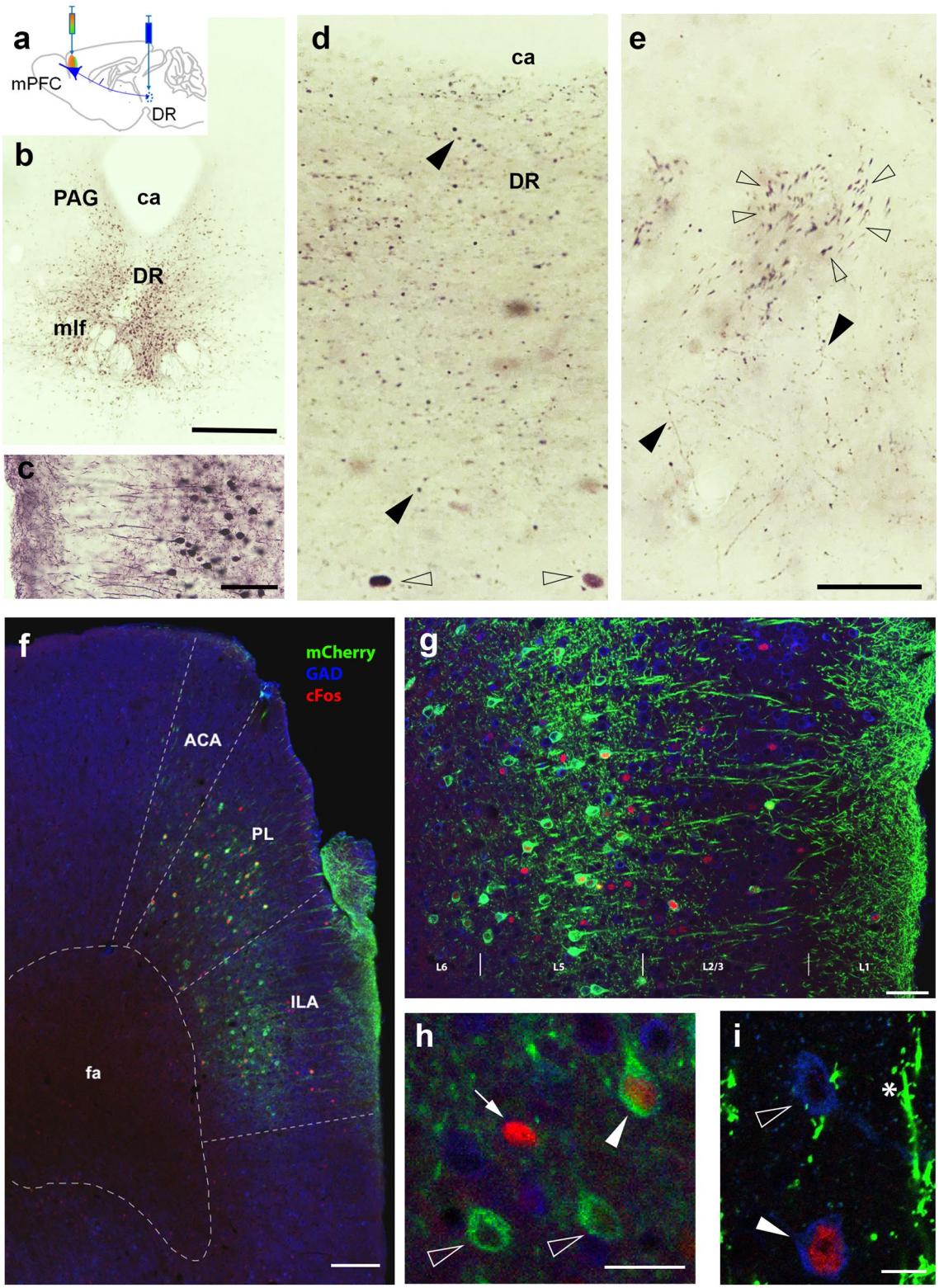

Brain tissue preparation for light and electron microscopy

Euthanasia was achieved by anesthetizing animals deeply using urethane (1000–1500 mg/kg, I.P.). The age of the animals ranged from P60 to P67 for both the DREADD and CON groups. For the DREADD animals, the day of euthanasia corresponded to be 1–3 days following the

◂**Fig. 3** Confirmation of DREADD expression in the mPFC→DR neurons and representative triple IF confocal images of mPFC neurons. **a** Schematic of the stereotaxic injection of AAVrg-EBFP-Cre into DR and of the cre-dependent DREADD-AAV into mPFC. **b** Verification of AAVrg-EBFP-Cre deposition into DR. Note that the region with the highest density of EBFP-immunoreactivity is in the DR. ca = cerebral aqueduct; PAG = periaqueductal gray; mlf = medial longitudinal fasciculus. Scale bar = 500 µm. **c** Verification of Gq-DREADD-mCherry expression in Layer 5 pyramidal neurons of the mPFC. mCherry-immunoreactivity is prevalent within cell bodies in Layer 5, apical dendrites traversing across Layers 2/3 and branching in Layer 1. The section was dually labeled using anti-cFos, resulting in immunoreactivity of nuclei of the same population of pyramidal neurons. Scale bar = 100 µm. **d** Verification of Gq-DREADD-mCherry expression in puncta of DR. Vibratome sections containing DR were processed in parallel with sections containing mPFC that is shown in panel (**c**). Puncta reflecting mCherry-immunoreactive axon terminals are evident in DR, ventral (filled arrowheads) and lateral to the cerebral aqueduct. Nuclei immunoreactive for cFos are also evident (open arrows) in DR. **e** Verification of Gq-DREADD-mCherry expression in axons coursing within fiber bundles of the internal capsule (open arrowheads) and varicose axonal processes (filled arrowheads) in dorsal striatum. Scale bar = 50 µm and applies to panels (**d**, **e**). **f** Overview of the section showing mCherry (green), cFos (red/magenta) and GAD (blue) immunofluorescence. Note that most of the mCherry signals were contained in the prelimbic (PL) and infralimbic (ILA) areas, which constitute major parts of mPFC. ACA, anterior cingulate area (also referred to as Cg1); fa, anterior forceps. Scale bar = 170 µm. **g** Laminar distribution of mCherry, cFos and GAD immunolabeling. Layers were identified according to Allen Brain Atlas based on the distance to pia: Layer 1, 0–125 µm; Layers 2/3, 125–325 µm; Layer 5, 325–525 µm; Layer 6, >525 µm. Scale bar = 50 µm; **h** Representative image of an mCherry+/cFos + neuron (filled arrowhead), mCherry+/cFos-negative neurons (open arrowheads), and an mCherry-negative/cFos + neuron (arrow). Scale bar = 25 µm; **i** Representative image of a GAD+/cFos + neuron (filled arrowhead), a GAD+/cFos-negative neuron (open arrowhead), and an mCherry + dendrite with spines (asterisk). Scale bar = 10 µm

last DREADD ligand injection during recovery. After confirming that animals showed complete absence of leg retraction to toe pinches following urethane injection, animals were transcardially perfused with the following solutions: saline buffered with 0.01 M phosphate buffer (PBS, pH 7.4) containing 10,000 units/500 ml of Heparin, followed immediately by 4% paraformaldehyde (PFA) buffered with 0.1 M phosphate buffer (PB, pH 7.4). All DREADD animals and all CON were euthanized in this way. Brains were extracted from the skull, then post-fixed in 4% PFA/0.1 M PB for at least three days at room temperature. Each brain was blocked and sectioned along the coronal plane at a thickness of 50 µm using a vibrating microtome. Brain sections from all DREADD animals ($N = 7$) and CON animals ($N = 11$) underwent this euthanasia protocol. All brain tissue from DREADD animals underwent immunocytochemical processing described in the following section, as did all but one of the brains of the 11 CON animals. Brain of one CON animal was excluded from image analysis, due to poor tissue preservation.

Verification of DREADD gene expression in the mPFC→DR pathway

Even though EBFP, mCherry and mCitrine are inherently fluorescent proteins, we employed immunocytochemistry to enhance detection of these reporter proteins.

Immunoreagents used The successful deposition of AAVrg-EBFP-Cre in DR was confirmed using a rabbit anti-GFP primary antibody (Invitrogen (Molecular Probes) Cat # A11122; RRID AB_221569, 1:2000), taking advantage of its cross-reactivity for detecting EBFP, followed by the use of a goat anti-rabbit IgG for the secondary antibody (Vector Cat # BA-1000 lot ZA-0924, 1:200) and Vector's Elite kit (PK-6100, Vector Laboratories) with VIP as the color indicator (SK-4605, Vector Laboratories) (Fig. 3a, b). This immunocytochemical procedure also detected mCitrine, the reporter of KORD (not shown). In sections semi-adjacent to those processed for EBFP detection, the expression of Cre-dependent Gq-DREADD genes was verified using a rat anti-mCherry primary antibody (ThermoFisher, Cat. No. M11217, RRID AB_2536611, 1:1000), a biotinylated goat anti-rat IgG secondary antibody (Vector Laboratories Cat #BA-9400, lot Z001216, 1:200) and Vector's Elite Kit with VIP as the indicator.

To verify that the pyramidal neurons with immunoreactivity to mCherry were activated by the DREADD ligand, C21, a subset of the sections immunolabeled for mCherry were also immunolabeled for cFos, an immediate early gene product that marks activated neurons (Bullitt 1990). To this end, vibratome sections were co-incubated with rat anti-mCherry and rabbit anti-cFos primary antibody (Cell Signaling Tech, Cat. No. 5348S; RRID AB_10557109, 1:800), followed by co-incubation in biotinylated goat anti-rat IgG and biotinylated goat anti-rabbit IgG (Vector Laboratories Cat# BA-1000, lot ZA-0924, 1:200) secondary antibodies, and visualized using the same kit as above. cFos versus mCherry-immunoreactivity could be distinguished by the nuclear location of cFos, in contrast to the perikaryal localization of mCherry.

VIP immunocytochemical procedure for bright-field light microscopy Vibratome sections were first incubated for 30 min with 1% H_2O_2 in 0.01 M phosphate buffer/0.9% sodium chloride (PBS) to eliminate background immunolabeling. This step eliminated the mCherry, mCitrine and EBFP fluorescence, so that the detection of the viral gene reporters became completely reliant on the secondary antibodies' signals. Sections were subsequently rinsed in PBS, then were blocked for 30 min in PBS buffer containing 1% bovine serum albumin (BSA) and 0.05% sodium azide. Incubations with the primary antibodies, anti-GFP and anti-mCherry occurred over a period of 1–3 days, under constant agitation at room temperature. Following three rinses in PBS, sections were incubated with the secondary antibodies

for 1 h at room temperature, under constant agitations. After this step, sections were processed for the ABC-peroxidase reaction by following the Vector Laboratories' User Guide. Sections were mounted on glass slides, coverslipped and visualized using the Echo Revolve light microscope.

Immunocytochemistry for triple immunofluorescence confocal microscopy to assess activation of Gq-DREADD-transfected cells and GABAergic interneurons simultaneously

To confirm that C21 activated Gq-DREADD-transfected pyramidal neurons in the mPFC, and to ascertain whether the firing of pyramidal neurons increased the firing of GABAergic interneurons (GABA-INs) in the mPFC, animals were injected with C21 approximately 90 min prior to euthanasia.

Tissue preparation, immunoreagents used and the immunocytochemical procedure Intact sections that contained cingulate cortex area (Cg1, also referred to as ACA), prelimbic cortex (PL) and infralimbic cortex (IL) (~Bregma 1.98–2.32 mm) of these DREADD gene-transfected ABA animals, together with vibratome sections prepared as described above for the control ABA animals without DREADD expression (CON, $N = 10$, 1 of the 11 CONs excluded from anatomical studies due to poor tissue preservation) underwent the immunocytochemical procedure. After incubating sections for 30 min with 1% H_2O_2 in PBS, sections were rinsed in PBS, then were blocked for 30 min in PBS buffer containing 1% BSA and 0.05% sodium azide. Sections were then incubated in PBS-BSA-azide containing three primary antibodies: rabbit anti-cFos antibody (Cell Signaling Tech, Cat. No. 5348S; RRID AB_2536611, 1:800), rat anti-mCherry antibody (ThermoFisher, Cat. No. M11217, RRID AB_2536611; 1:1000), and mouse anti-glutamic acid decarboxylase 67 (GAD) antibody (Millipore Sigma, Cat. No. MAB5406, clone 1G10.2; RRID AB_2278725, 1:800). After one to three days of incubation at room temperature, brain sections were washed three times with PBS for ten minutes each. Sections then were incubated in PBS-BSA-azide buffer containing the following secondary antibodies: goat anti-rat IgG antibody conjugated to Alexa Fluor 594 (Jackson ImmunoResearch, Cat. No. 112-585-143; 1:100) to recognize anti-mCherry, Affini-pure goat anti-rabbit IgG antibody conjugated to Alexa Fluor 647 (Jackson ImmunoResearch, Cat. No. 111-605-144; 1:100) to recognize anti-cFos, and goat anti-mouse IgG antibody conjugated to DyLight 405 (Jackson ImmunoResearch, Cat. No. 111-475-166,1:100) to recognize anti-GAD. After an overnight incubation in secondary antibodies at room temperature, brain sections were washed three times with PBS for 10 min each.

Controls for immunofluorescence microscopy We routinely conducted two types of controls. One was to stain sections singly, to ensure no 'bleeding' of fluorescent labels beyond the channel designated for the immunolabeling. The second was to pair a primary antibody with a secondary antibody of an inappropriate species, to ensure absence of inter-species cross-reactivity.

Confocal microscopic imaging and analysis Two brain sections from each animal, containing IL PL and Cg1, were analyzed under the confocal microscope Leica Confocal SP8 with Leica's Application Suite 2.6.0 using three channels to visualize three kinds of secondary antibodies separately. From brain sections of each animal, 3–7 non-overlapping images, each approximately 581 × 581 µm, resolution of 1024 × 1024 pixels, at optical section thickness setting of 0.2 µm were taken from the mPFC using a 20× objective. Region of interest (ROI) spanning pial surface to deep Layer 5 was selected and its area measured using ImageJ (version 1.52K; RRID: SCR_003070, National Institute of Health, USA). Table 1 lists the exact values of the total area in μm^2 and the number of non-overlapping ROIs sampled from each animal.

Image J was also used to count immunolabeled cells in the images taken from the three channels of the confocal microscope. For each image, a window containing Cg1, PL and/or IL cortex was selected. Every neuron excluding those lying on the bottom or the right border of this window was

Table 1 Total area and number of ROIs sampled by confocal microscopy

Animal ID	Area sampled for IF (μm^2)	No. of fields analyzed for IF
DREADD-expressing		
275,172	1,322,034	7
275,176	1,342,383	7
278,874	768,627	4
278,875	1,192,348	6
278,876	1,156,409	6
285,264	838,357	5
285,366	988,962	5
CON		
269,406	0	0
270,322	528,857	4
273,435	525,731	4
273,437	784,097	6
275,175	693,635	4
275,177	509,392	3
278,092	630,842	4
278,093	496,448	4
278,871	516,747	3
278,872	521,475	3
285,257	706,239	4

counted and its distance to the pial surface was measured. Every neuron with florescence detected by the mCherry channel was treated as a mCherry+ (i.e., Gq-DREADD-expressing) neuron (shown by pseudocolor green in Fig. 3f). Only those neurons with ring-shaped labeling detected in the GAD channel was categorized as GAD + (i.e., GABA-IN). For the cFos channel, optical density of the nucleus of each labeled neuron was measured. From the histogram, it was determined that cFos intensity greater than 25 or the ratio of cFos intensity divided by the mean value intensity in a single window greater than 0.5664 was regarded to be above the threshold of cFos+ (i.e., activated).

Immunohistochemistry and tissue processing for electron microscopy

Brain sections from the DREADD group ($N = 7$) that were semi-adjacent to the vibratome sections used for immunofluorescence microscopy were used for electron microscopic analyses. Each section underwent freeze–thawing (Wouterlood and Jorritsma-Byham 1993) to increase the permeability of cell membranes with minimal disturbance of membranous structures. The immunohistochemistry procedure for dual labeling of GAD and mCherry began by blocking nonspecific immunolabeling by incubating for 30 min in 0.01 M PBS/0.05% azide/1% BSA. This was followed by a three days' primary antibody incubation in rat anti-mCherry antibody (ThermoFisher, Cat. No. M11217; RRID AB_2536611, 1:1000) and mouse anti-GAD antibody (MilliporeSigma, Cat. No. MAB5406; RRID AB_2278725, 1:800) diluted in pH 7.6 PBS-BSA-azide. This was followed by an overnight incubation in PBS-BSA-azide containing Ultra-small colloidal gold-conjugated goat anti-rat secondary antibody (1:100, EMSciences Hatfield, PA Cat 25181) and biotinylated goat anti-mouse secondary antibody (1:200, Vector Labs BA-1000). After that, sections underwent 30 min of incubation in avidin-biotinylated horseradish peroxidase complex formation (ABC, Vector's ABC Elite kit), then 15 min of post-fixation using 2% glutaraldehyde in PBS, then the steps for silver intensification (KPL Silver Enhancer Kit, Cat # 5520-0021) to enlarge the Ultra-small colloidal gold particles conjugated to anti-rat IgG, then finally of incubation of tissue in 3,3'- diaminobenzidine (DAB, Sigma Chem., Cat # 5905) substrate to develop the ABC-HRP-DAB reaction product. The EM tissue processing was similar to the procedure performed before (Chen et al. 2016), which consisted of post-fixation using 0.1% osmium tetroxide/0.1 M phosphate buffer processing for 30 min, followed by osmium-free tissue processing in 1% tannic acid, 1% uranyl acetate and 0.2% iridium tetrabromide, each dissolved in maleate buffer (pH 6.0, 0.1 M), post-fixation in 1% uranyl acetate in 70% ethanol (EtOH) overnight, dehydration in 70%/90%/100% EtOH and 100% acetone, infiltration in EPON 812 (EM Sciences), flat-embed between Aclar plastic sheets (EMSciences) and capsule-embedded in BEEM capsules (EMSciences). Ultrathin sections were prepared using the Ultracut E ultratomicrotome and collected on nickel grids (EMSciences). Lead citrate counterstaining was omitted, so as to facilitate detection of HRP-DAB reaction products.

Electron microscopic imaging and analysis The imaging window under the electron microscope (EM, JEOL 1200 XL, Tokyo) was confined to Layer 5 of mPFC (PL, IL and Cg1) and each window was required to contain at least two cell bodies with silver-intensified gold particles overlying the plasma membrane and/or in the cytoplasm (mCherry + neurons). Images were captured at a magnification of 10,000×–40,0000×, using the Hamamatsu CCD camera (1.2 megapixel) and software from AMT (Boston, MA, USA). The GABAergic terminals were distinguished from other axon terminals based on their HRP/DAB reaction produce appearing more electron dense than mitochondria and postsynaptic densities in the immediate vicinity.

For each animal, approximately 10 mCherry+ and 10 mCherry-negative pyramidal neurons were sampled and quantified. Neurons were identified to be pyramidal, based on the smooth contour of the nuclear membrane, unlike GABA-INs that exhibited deep invaginations of the nuclear membrane. Pyramidal neurons were considered to be mCherry-positive when 2 or more SIG particles could be detected along a 1 µm segment plasma membrane. A neuronal cell body was considered to be mCherry-negative when SIG particles occurred only in the nucleoplasm and/or the density of SIG particles was less than 1/50 of that identified along the plasma membrane of a nearby mCherry + neuron. GABAergic terminals that were aligned in parallel with the plasma membrane of the cell body were identified to be forming inhibitory synapses. Synapse length was measured using the segmented lengths tool of ImageJ (version 1.52 k). The lengths spanning the plasma membrane adjacent to GABAergic terminals were also measured using the same ImageJ software.

Statistical analyses

Statistical analyses were performed using GraphPad Prism versions 8 or 9.2.0 Normality tests were followed by *t*-tests, one-way ANOVA or nonparametric tests, and simple linear regressions of correlation.

Image processing for preparation of figures

Images captured by the confocal microscope and electron microscope were cropped, resized and matched for contrast and brightness using Adobe Photoshop.

Results

Wheel running, food intake and body weight during ABA1

Nine out of 18 (5 out of 7 DREADD; 4 out of 11 CON) animals increased their daily 24-h wheel running progressively during the acclimation phase of ABA1, when animals had access to a wheel without food restriction (FR) (Pre3 to Pre1, Fig. 1a, b). Following commencement of FR on FR1, 13 out of 18 (5 out of 7 DREADD; 8 out of 11 CON) animals increased their wheel running during the hours of 4 PM–7 PM that preceded the hours of food availability (FA) of 7 PM–9 PM. This increase during the hours of 1 PM–7 PM, often referred to in the literature as the food anticipatory activity (FAA) (Hall et al. 1953) was significantly different during ABA1, relative to values during the acclimation days, Pre1 and Pre2 ($p = 0.0237$, paired t test, Fig. 1c). All animals survived three days of FR, in spite of having lost 23%, on average, of their body weight at the end of ABA1, calculated as follows: Body weight on FR1, FR2 and FR3, normalized to the pre-FR body weight at 1 PM. (Fig. 1d). This was due to the reduction of daily food intake by 70%, calculated as the difference in the averaged value of food intake during two pre-FR days relative to the averaged value of food intake during three FR days, normalized to the averaged value of food intake during two pre-FR days) (shown as changes in kcal consumed in Fig. 1e). Within 24 h of having returned to ad libitum food availability, their body weights were restored to pre-FR values (Fig. 1d). We also observed a significant decrease in the post-ABA (average of post-FR days 1 and 2) food intake in the DREADD group compared to CONs (Fig. 1e), but this difference disappeared as recovery continued, so that food intake immediately preceding ABA2 became similar between the two groups (Fig. 2d). Overall, these observations indicated that most animals of both the DREADD and CON groups responded to FR with significant elevation of wheel running, although a few from both groups did not.

Wheel running, food intake and body weight during ABA2

Following ABA1, all animals were returned to an environment with ad libitum food availability and no wheel for 6 days. At the end of the recovery phase, a wheel was returned to each animal's cage to allow for re-acclimation (Pre4 to Pre1). At the end of the re-acclimation phase of ABA2, all of the animals resumed or surpassed the level of wheel running observed by the end of the acclimation phase of ABA1 (Fig. 2b, c). Following commencement of FR on FR1 of ABA2, 5 out of 18 animals (2 out of 7 DREADD and 3 out of 11 CON) increased their wheel running during the hours preceding the feeding hours of 7 PM–9 PM. By FR2, this increase reached significance (4 out of 7 DREADD and 8 out of 9 CON, wheel data acquisition for 2 CON animals failed transiently), relative to the average running during the hours of 4 PM–7 PM on Pre2 and Pre1 days that preceded FR ($p = 0.04577$, paired t test, Fig. 2c). All animals survived four days of FR, in spite of having reduced food intake by 60% (expressed in kcal food intake in Fig. 2d) and lost 21% of their body weight (Fig. 2c). Within 24 h, their body weights were restored to pre-FR values (Fig. 2c). These observations indicate that the majority of the animals of both the DREADD and CON animals increased wheel running significantly, following multiple days of FR but included a few that did not.

The effect of C21/Gq-DREADD activation and SalB/KORD-DREADD inhibition of mPFC→DR neurons on wheel running

At 3:30 PM and 9:30 PM on FR2 of ABA2, all animals of the DREADD group received 1 mg/kg of C21 by intraperitoneal injections (Fig. 2a). Comparisons of wheel running of animals transfected with Gq-DREADD in mPFC versus the CONs without Gq-DREADD transfections revealed no group difference on FR2 during the 3 h preceding feeding (FAA, 4 PM–7 PM, Mann–Whitney test, mean ± SD of 1.064 ± 1.120 km for the DREADD group; 0.654 km ± 1.034 km for CON group, Mann–Whitney $U = 23.50$, $p = 0.4240$), during the 2 h of food availability (FA, 7 PM–9 PM, mean ± SD of 0.910 ± 0.918 km for the DREADD group, 0.674 ± 0.380 km for the CON group, Welch's t test, $p = 0.5413$), or postprandially (PP, 9 PM–1 AM, mean ± SD 5.082 ± 0.899 km for the DREADD group; 4.712 ± 1.904 km for the CON group, Welch's t test, $p = 0.6170$) (Fig. 2b). The average wheel running during the 2 h post-injection of C21 (4 PM–6 PM) also did not reveal any group difference (mean ± SD 0.417 ± 0.584 for the DREADD group; 0.209 ± 0.479 for the CON group, Mann–Whitney test, $p = 0.3247$).

At 3:30 PM and 6:30 PM on FR4 of ABA2, all animals of the cohort received 10 mg/kg of SalB by intraperitoneal injections to suppress activity of the mPFC→DR pyramidal neurons (Fig. 2a). No significant difference in wheel running on FR4 was found during 3 h preceding feeding (FAA, 4 PM–7 PM, mean ± SD of 0.681 ± 1.134 km for the DREADD group; 1.364 ± 2.010 km for the CON group, Mann–Whitney test, $p = 0.1854$), during the 2 h following the first injection of the DREADD ligand (4 PM–6 PM, mean ± SD of 0.658 ± 1.091 km for the DREADD group and 0.759 ± 1.489 km for the CON group,

Mann–Whitney test, $p = 0.6907$), during the 2 h of food availability (FA, mean ± SD of 0.172 ± 0.209 km for the DREADD group and 0.217 ± 0.161 km for the CON group, Welch's t test, $p = 0.6403$) or PP (9 PM–1 AM, mean ± SD of 2.208 ± 1.711 km for the DREADD group and 3.154 ± 1.921 km for the CON group, Welch's t test, $p = 0.2942$) (Fig. 2b).

To assess whether C21 or SalB might alter wheel running of sated animals, the same dose of the ligands were administered during the recovered phase following ABA2. We detected no difference in wheel running during any of the hours between the DREADD and CON groups (Fig. 2c). After C21 was administered to weight-recovered mice, we observed no differences between DREADD and CON groups in running during FAA (mean ± SD 0.1243 ± 0.1771 km for DREADD, 0.0330 ± 0.0508 km for CON; Welch's t test, $p = 0.229$), FA (mean ± SD 2.852 ± 0.9916 km for DREADD, 2.943 ± 1.308 km for CON; unpaired t test, $p = 0.8803$), or PP time bins (mean ± SD 3.862 ± 3.416 km for DREADD, 4.120 ± 2.887 km for CON; unpaired t test, $p = 0.8722$). Likewise, after SalB was administered to weight-recovered mice, we observed no differences between DREADD and CON groups in running during FAA (mean ± SD 0.0978 ± 0.1960 km for DREADD, 0.0451 ± 0.0314 km for CON; Welch's t test, $p = 0.5062$), FA (mean ± SD 1.620 ± 1.114 km for DREADD, 2.041 ± 1.241 km for CON; unpaired t test, $p = 0.4843$), or PP time bins (mean ± SD 3.826 ± 2.885 km for DREADD, 4.557 ± 2.318 km for CON; unpaired t test, $p = 0.5705$).

These findings indicated that group mean values of wheel running were not significantly altered by the chemogenetic activation or suppression of PFC→DR neurons. The relatively large variance was likely to have occluded chemogenetic modulations of any individual.

The effect of C21/Gq-DREADD activation and SalB/KORD-DREADD inhibition of mPFC→DR pyramidal neurons on food consumption

Previous studies uncovered that mPFC→DR pyramidal neurons project mostly to the GABA-INs in DR (Jankowski and Sesack 2004), and that direct activation of those inhibitory neurons in DR promotes food intake (Nectow et al. 2017). Thus, we predicted that C21/Gq-DREADD activation of mPFC→DR neurons would promote feeding during the limited hours of food availability on FR2 of ABA2. Contrary to this expectation, activation of mPFC→DR pyramidal neurons yielded no significant difference in the group mean value of feeding by the DREADD group, compared to the control ABA animals without activation of DREADDs (mean ± SD 3.997 ± 0.932 for DREADD, 4.406 ± 0.565 for CON Welch's t test, $p = 0.3240$) (Fig. 2d). SalB/KORD-DREADD inhibition of mPFC→DR neurons on FR4 of ABA2 also did not yield significant differences in the group mean value of food intake across the DREADD versus control groups (mean ± SD 3.856 ± 1.490 for DREADD, 3.626 ± 1.067 for CON, Mann–Whitney test, $p = 0.2854$) (Fig. 2d).

Thus, food consumption, like wheel running was not significantly altered by chemogenetic modulation in either direction.

Rationale for the anatomical experiments

Although chemogenetic modulation of the mPFC→DR pyramidal neurons did not yield statistically significant group mean differences in wheel running or food consumption, relative to controls lacking the expression of DREADDs, we noted substantial individual differences in these behaviors. To verify that DREADD did modulate neuronal activity and to assess whether individual differences in behavior might be related to individual differences in the microcircuitry of the mPFC activated by C21, we first confirmed that DREADD genes were expressed in mPFC pyramidal neurons, including their axon terminals of DR, then quantified the proportion of C21-activatable mPFC neurons by immunofluorescence.

Confirmation of DREADD expression in mPFC pyramidal neurons and DR axons by immunocytochemistry

Immunocytochemistry was performed to verify successful targeting of DR for viral injection. EBFP, the reporter protein of the retrogradely transported AAV expressing the Cre protein (AAVrg-EBFP-Cre, Fig. 3a, b) was expressed at high density within neurons located in DR, where the virus was aimed for stereotaxic injection (Fig. 3b). The Cre-dependent expression of DREADD genes in the perikaryal cytoplasm and dendrites of mPFC pyramidal neurons was verified by the immunoreactivity of these cells to the reporter protein, mCitrine, of KORD (not shown) and of the reporter protein, mCherry of Gq-DREADD (Fig. 3c, f). High density of axon terminals with immunoreactivity to mCherry were evident in DR (Fig. 3d) as were axons with immunoreactivity to mCitrine (not shown). As expected (Anastasiades and Carter 2021), a much lower density of fine-caliber, varicose axon terminals, presumably axon collaterals of mPFC pyramidal neurons projecting to the pyramidal tract, were detected within the medial subregion (i.e., near the lateral ventricles) of dorsal striatum, among immunoreactive fiber bundles of the internal capsule (Fig. 3e).

Validation of the C21-activation of Gq-DREADD-expressing neurons in Layer 5 of mPFC within tissue immunolabeled triply for mCherry, cFos and GAD

Brain sections containing mPFC were examined under the confocal microscope after immunohistochemical processing. Representative images are shown in panels f–i of Fig. 3. The expression of mCherry-tagged Gq-DREADDs in perikaryal cytoplasm was localized to Layer 5 and mainly confined in the prelimbic and infralimbic areas (Fig. 3f). This laminar pattern in cortex was as expected, based on the known laminar distribution of mPFC pyramidal neurons with projections to DR (Jankowski and Sesack 2004) as well as the targeted locations of stereotactically injected rgAAV-EBFP-Cre virus in DR and of the Cre-dependent AAV-DREADD in cerebral cortex. At a higher magnification, the mCherry-tagged Gq-DREADD-expressing cells were verified to be pyramidal neurons based on their long singular apical dendrites spanning through Layers 2/3 and 1 of mPFC (Fig. 3g), and by the prevalence of dendritic spines (white asterisk, Fig. 3i).

Besides mCherry, sections were co-labeled for the immediate early gene product, cFos, an indicator of neuronal firing, and glutamic acid decarboxylase (GAD), a synthetic enzyme for GABA and thus an indicator of GABAergic inhibitory neurons (GABA-IN). As shown in Fig. 3g, h, cFos immunoreactivity was restricted to the nucleus, which conforms to the expression and the nuclear translocation of cFos protein upon neuronal firing (Bullitt 1990; Roux et al. 1990). GABA-IN were identified by GAD immunoreactivity exclusively within the cytoplasm and their relatively small cell body diameter (Fig. 3f). Although there is a previous report of GABAergic neurons in mouse frontal cortex projecting to DR (Tomioka et al. 2015), GAD immunoreactivity was absent among the mCherry + neurons of our preparations (Fig. 3g, h), confirming that mCherry + neurons in mPFC were pyramidal. A subpopulation of both the mCherry-expressing and GAD-immunoreactive neurons were cFos-immunoreactive (cFos+).

Together, these observations indicated that Gq-DREADD-expressing cells were conforming to the characteristics of Layer 5 pyramidal neurons reported to belong to those projecting to DR and lacking GAD immunoreactivity. Moreover, a subpopulation of both the Gq-DREADD-expressing neurons and GAD-immunoreactive neurons could be found to have been active within 90 min of C21 administration.

Laminar distributions of mCherry+, cFos+ and GAD+ neurons

The laminar distributions of mCherry+, cFos+ and GAD+ neurons (Fig. 4a) were assessed quantitatively and separately by calculating the relative fraction of the indicated cell type within 50 µm bins centered at a position specified by its distance to the pial surface. As shown in Fig. 4b, ~80% of the total mCherry+ neurons were located within 325–525 µm from pial surface, corresponding to Layer 5, as was expected (Jankowski and Sesack 2004).

The cFos laminar distributions were assessed for both the DREADD and CON groups (Fig. 4b). For the DREADD group, most of the cFos + neurons were located around 400 µm to pia, which coincided with the pinnacle of the distribution of mCherry + neurons (Fig. 4b). For the CON group, however, cFos + distribution showed a smaller fraction at around 400 µm from pia but a relatively greater fraction around Layer 2/3 (Fig. 4b). This indicates that C21 effectively drove neuronal firing in Layer 5, where most of the Gq-DREADDs were expressed. Interestingly, while less than 13% of the mCherry + neurons were distributed at around 125–325 µm, corresponding to Layers 2/3, the fraction of cFos + neurons within the same layer of the DREADD group accounted for as much as ~34% of the total cFos + population (Fig. 4b). This indicates that neurons in Layers 2/3 were also activated, although unlikely by direct Gq-DREADD-mediated modulation.

As for the GAD+ neurons, their laminar distributions in the DREADD and the CON groups were similar (Fig. 4c): both peaked within Layer 1 and were relatively evenly distributed across the deeper layers.

Together, these observations indicated that C21 primarily drove PFC→DR pyramidal neurons in layer 5 but that this activation also recruited activity of neurons in Layers 2/3.

Density of cFos+ neurons is increased by C21/Gq-DREADDs in Layers 5 and 2/3

For both the DREADD and the CON groups, the cFos + neuronal density in mPFC was calculated within 50 µm-wide windows along the laminae of mPFC and centered at a position specified by their distance to pial surface, as described above for the laminar distribution of the three cell types (Fig. 5a). The value of cFos+ neuronal densities across at varying distances from pia were averaged across ~4 confocal microscope windows for each animal. Across laminar distances ranging from 200 to 550 µm from pia (Layer 2 through the start of Layer 6), the cFos+ neuronal density was significantly greater for the DREADD group than the CON group (Fig. 5b). The cFos + densities in Layers 2/3 and 5 were both significantly greater for the DREADD group than CON group (Fig. 5c, mean ± SD 0.688 ± 0.443 for DREADD Layers 2/3, 0.250 ± 0.201 for CON Layers 2/3, Mann–Whitney $U = 6.000$, $p = 0.003085$ for Layers 2/3; mean ± SD 1.139 ± 0.523 for DREADD Layer 5, 0.290 ± 0.225 for CON Layer 5, Mann–Whitney $U = 3.000$, $p = 0.000720$ for Layer 5). These results further reveal that C21/Gq-DREADDs elevated the activities not only of Layer 5 neurons but also of Layer 2/3 neurons.

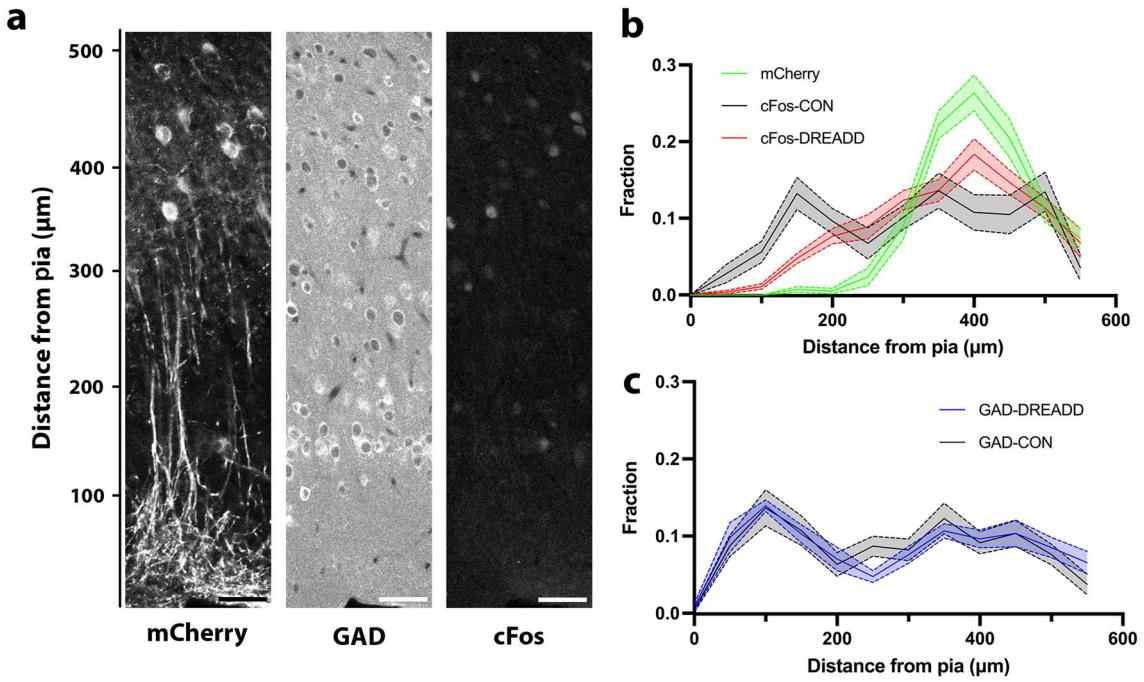

Fig. 4 Laminar distributions of mCherry+, GAD+and cFos+neurons. **a** The same window within IL from a DREADD experimental animal captured by GAD, mCherry and cFos immunofluorescence channels, respectively. Pial surface is located at the very bottom of the image. Scale bars = 50 µm. **b** The fraction of mCherry+and cFos+neurons distributed across laminae for the DREADD group ($N = 7$) and the CON group ($N = 10$). **c** The fraction of GAD+neurons distributed across the laminae for the DREADD group ($N = 7$) and the CON group ($N = 10$). Each data point represents the relative fraction of the indicated cell type within a 50 µm bin centered at the position specified by its x-coordinate. Data are shown as mean ± SEM

Activities of GABAergic neurons

The cFos+density quantification described above did not differentiate GABAergic versus pyramidal neurons. The activities of the GABAergic subset of neurons in mPFC were examined through immunofluorescence as well. For each animal, we calculated the averaged percentage of GAD+neurons that co-expressed cFos (%GAD+/cFos+, Fig. 3f) captured from all windows that covered mPFC layers. The %GAD+/cFos+for the DREADD group was significantly greater than that for the CON group (Fig. 6a; mean ± SD 7.7 ± 4.7% for DREADD, 2.2 ± 1.9% for CON, Welch's $t_{(7.407)} = 2.937$, $p = 0.0205$). Notably, in the mPFC of DREADD animals, %GAD+/cFos+showed a positive correlation with the percentage of mCherry+neurons that co-expressed cFos (%mCherry+/cFos+, Fig. 6b). This correlation was nearly significant ($r^2 = 0.5507$, $p = 0.0562$).

Laminar analysis of the cFos+/GAD+cells revealed that Gq-DREADD activation increased the firing of GABA-IN across Layers 2/3 and 5 of the DREADD group more than of CONs (Fig. 6c; mean ± SD 0.034 ± 0.029 per 1000 µm^2 for DREADD Layers 2/3, 0.005 ± 0.008 per 1000 µm^2 for CON Layers 2/3, $p = 0.0203$ and Mann–Whitney $U = 12.00$ for Layers 2/3; 0.060 ± 0.038 per 1000 µm^2 for DREADD Layer 5, 0.014 ± 0.012 per 1000 µm^2 for CON Layer 5, $p = 0.010$ and Mann–Whitney $U = 9.5$ for Layer 5).

The great majority of the cFos+/GAD-negative cells were presumed to be pyramidal. This category of neurons in Layers 2/3 and 5 were also of higher density for the DREADD animals than for the CON animals (Fig. 6c; mean ± SD 0.654 ± 0.418 per 1000 µm^2 for DREADD Layers 2/3, 0.245 ± 0.201 per 1000 µm^2 for CON Layers 2/3, $p = 0.0068$ and Mann–Whitney $U = 8.000$ for Layers 2/3; 1.079 ± 0.496 per 1000 µm^2 for DREADD Layer 5, 0.277 ± 0.223 per 1000 µm^2 for CON Layer 5, $p = 0.0012$ and Mann–Whitney $U = 4.00$ for Layer 5). Moreover, among the cFos+cells, those that were both GAD-negative and mCherry-negative in Layer 5 were also more prevalent in the mPFC of DREADD animals than of the CON animals (0.789 ± 0.457 per 1000 µm^2 for DREADD Layer 5, 0.277 ± 0.223 per 1000 µm^2 for CON Layer 5, $p = 0.0031$, Mann–Whitney $U = 6.00$). These in the DREADD group were presumed to include the pyramidal neurons without projections to DR.

Overall, these observations indicate that GABA-INs, pyramidal neurons of Layers 2/3, and pyramidal neurons in Layer 5 without projections to DR were all driven to fire more, via the Gq-DREADD activation of mPFC→DR pyramidal neurons.

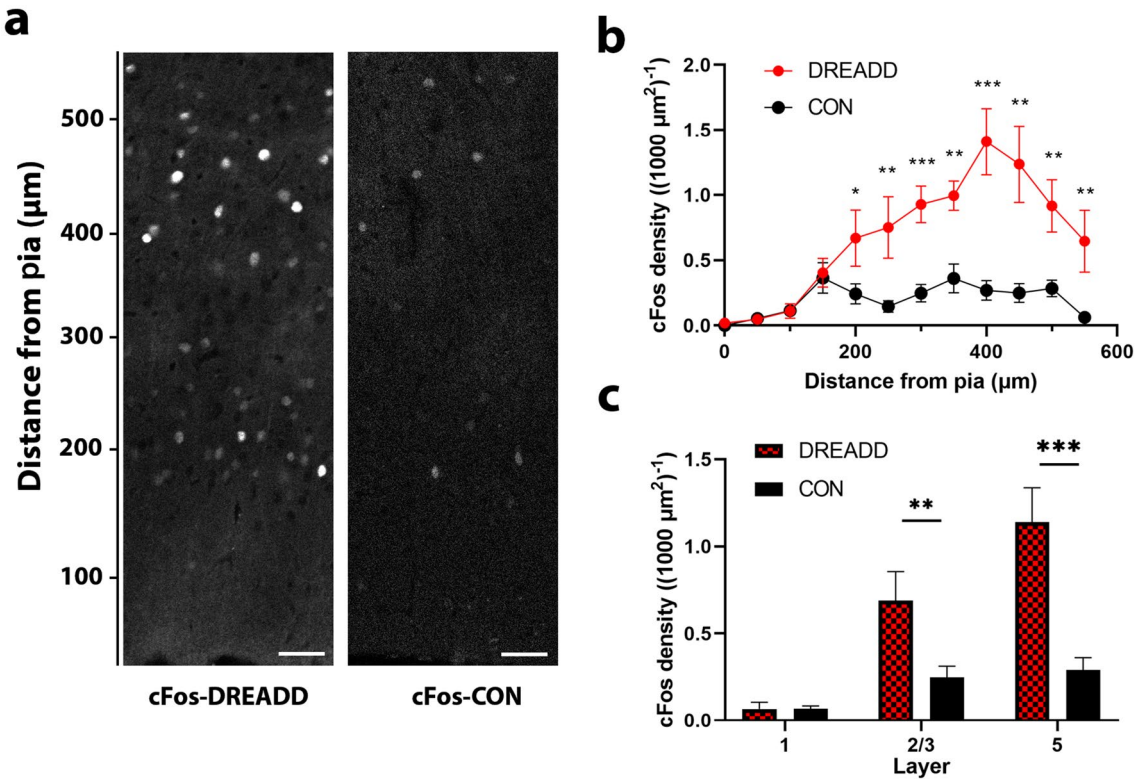

Fig. 5 cFos + neuron density across the laminae. **a** Representative confocal images showing cFos + neurons in PL across laminae of a DREADD group animal and a CON group animal. Pial surface is located at the very bottom of the image. Scale bars = 50 μm. **b** The density of cFos + neurons across the laminae. Each data point represents the density of cFos + neurons in a window centered at the position specified by its *x*-coordinate. The height of the quantified window was 50 μm while the width of the windows ranged from 300 to 400 μm, covering PL and/or IL. Data are shown as mean ± SEM. **c** The density of cFos + neurons by layers. Layer categorization was as described in Fig. 3. $*p \le 0.05$, $**p \le 0.01$, $***p \le 0.001$, $****p \le 0.0001$ by the Mann–Whitney test

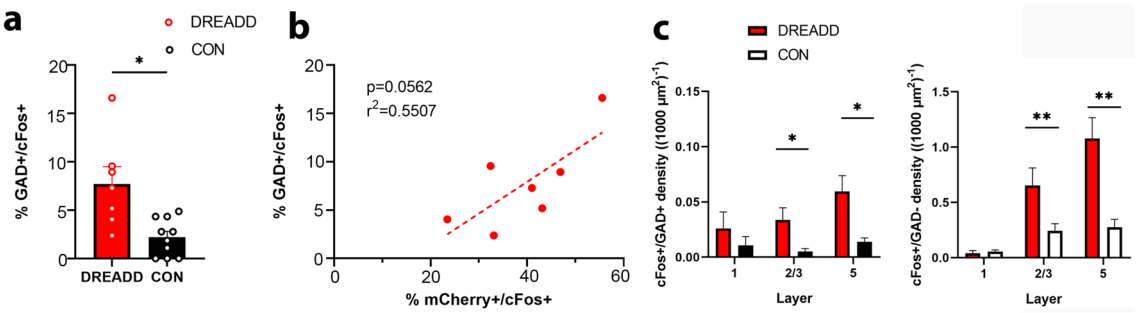

Fig. 6 **a** The percentage of GAD+/cFos+ neurons across all layers of the DREADD group ($N = 7$) and the CON group ($N = 10$). Each data point represents the average value of an animal. Data are shown as mean ± SEM. **b** Correlation between %GAD+/cFos+ and %mCherry+/cFos+ in the mPFC of DREADD group animals. Dashed line indicates correlation close to significance. **c** Distribution of the GAD+/cFos+ neurons across the layers (left) and of the cFos + /GAD-negative neurons across the layers (right). $*p \le 0.05$ and $**p \le 0.01$ by the Mann–Whitney test

Electron microscopic validation of Gq-DREADD expression in Layer 5 pyramidal neurons

EM imaging combined with immunocytochemistry enabled ultrastructural localization of mCherry-tagged Gq-DREADDs. As shown in Fig. 7, mCherry-immunoreactivity was on the plasma membrane and in the cytoplasm of Layer 5 mPFC pyramidal neurons' cell bodies (Fig. 7a), apical dendrites (Fig. 7b), and spine heads forming excitatory synapses (Fig. 7c). Together with Fig. 3, these results confirm the expression of Gq-DREADDs and their wide localizations within Layer 5 pyramidal neurons in the mPFC.

Electron microscopic analysis reveals more prevalent GABAergic innervation of mPFC→DR pyramidal cells than of neighboring Layer 5 pyramidal cells without projections to DR

GABAergic innervation of Layer 5 pyramidal neurons in the mPFC of the DREADD group was quantified in two ways: the percentage of plasma membrane covered by GABAergic terminals (%GABA innervation) and the number of GABAergic terminals per unit plasma membrane length (GABA Terminal Density) (Fig. 8a). The quantification was done for both mCherry + neurons and mCherry-negative pyramidal neurons in Layer 5 of mPFC. Neuronal cell bodies were verified to be pyramidal, based on the smooth contour of the nuclear membrane (White 1989) and lack of GAD immunoreactivity. Both measurements were significantly greater for the mCherry + pyramidal neurons than for the mCherry-negative pyramidal neurons within individual DREADD experimental animals (Fig. 8b) (paired t test, $t_{(6)} = 3.723$, $P = 0.0098$ for % GABA; paired t test, $t_{(6)} = 6.932$, $p = 0.0004$ for GABA Terminal Density). The greater %GABA innervation of mCherry + neurons was not due to differences in the lengths of individual GABAergic terminals (Kolmogorov–Smirnov $D = 0.08214$, $p = 0.2392$), but due to a significant decrease in their inter-synaptic lengths (Kolmogorov–Smirnov $D = 0.1298$, $p = 0.0102$) (Fig. 8c).

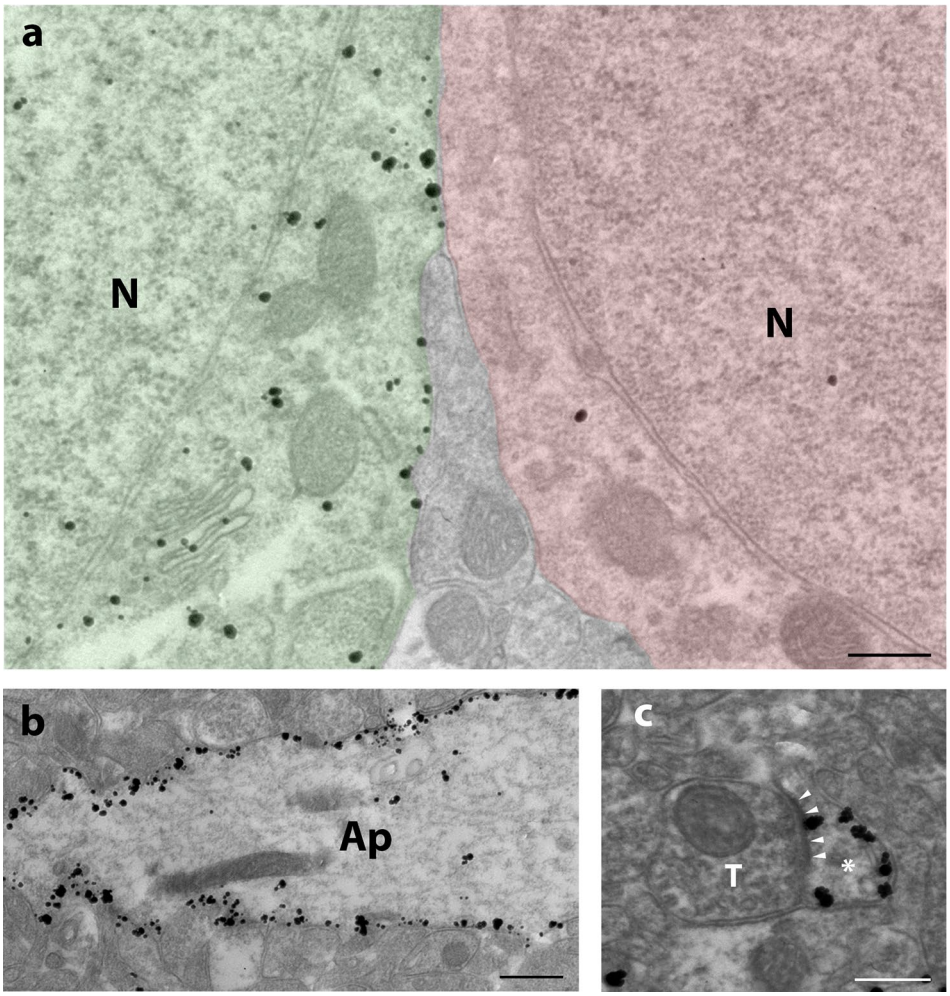

Fig. 7 Electron microscopic validation of the presence of Gq-DREADDs on neurons. **a** DREADD molecules labeled by silver-intensified gold (SIG) particles were present on the plasma membrane and in the cytoplasm of Layer 5 mPFC pyramidal neurons' cell body (green). The plasma membrane of an adjacent non-transfected pyramidal neuron with almost no Gq-DREADD-mCherry-immunoreactivity is shown on the right (red). *N* = nucleus. Scale bar = 500 nm. **b** SIG, reflective of Gq-DREADD/mCherry, on the plasma membrane of an apical dendrite (Ap). Scale bar = 1 µm. **c** SIG, reflective of Gq-DREADD/mCherry, along the plasma membrane of a dendritic spine head (white asterisk) forming an excitatory synapse with thick postsynaptic density (white arrowheads). Scale bar = 300 nm. T, axon terminal

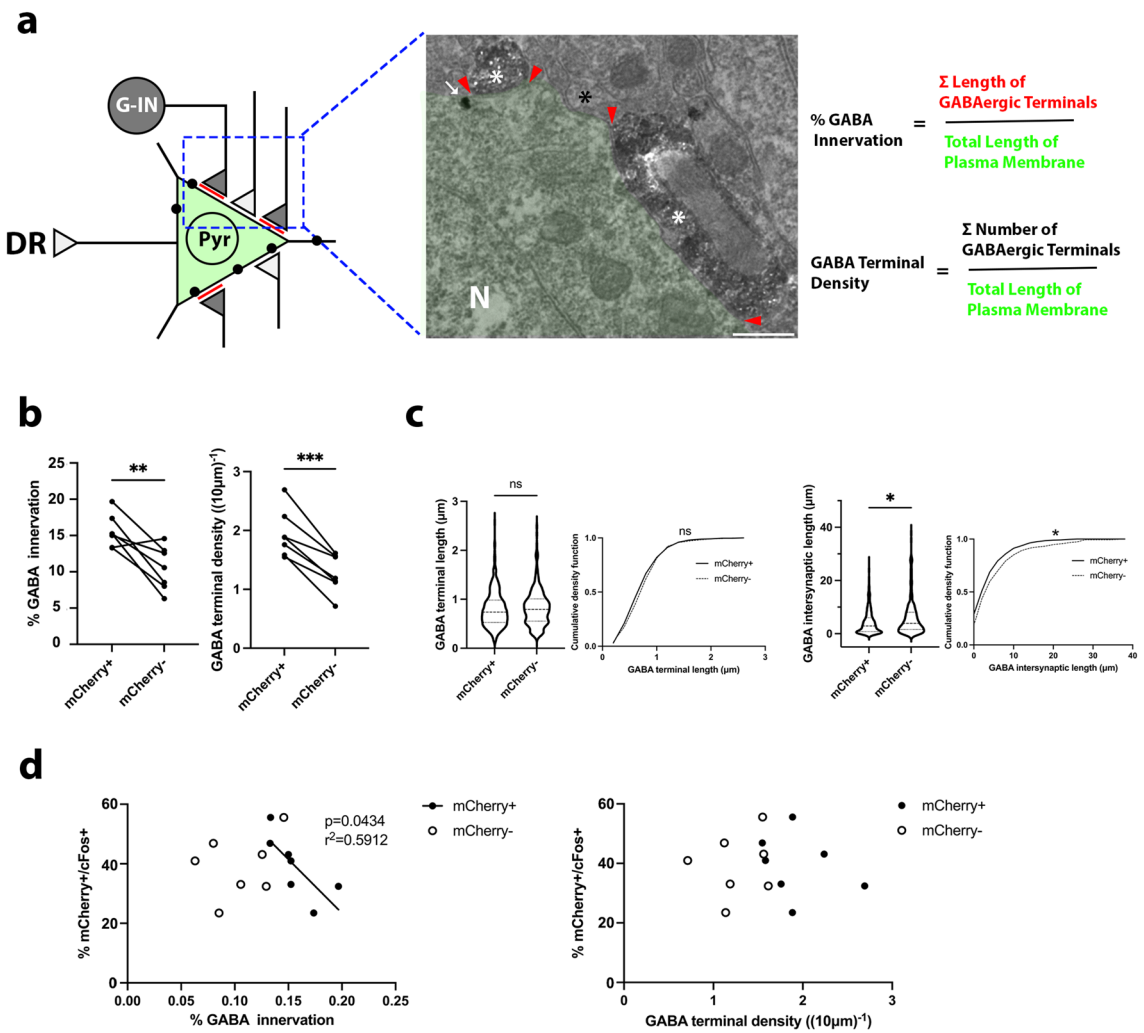

Fig. 8 Electron microscopic quantification of GABAergic innervation of mCherry + and mCherry-negative neurons' cell bodies in Layer 5 of mPFC. **a** Schematic illustration for the quantification of GABAergic innervation. Left, a cartoon showing an mCherry + pyramidal (Pyr) neuron labeled by silver-intensified gold particles (black dots). The GABAergic terminals (dark triangles) from the interneurons (G-IN) are distinguished from the other terminals (light triangles) due to the HRP-DAB reaction product indicating the presence of GAD. The cartoon does not reflect the relative size of a neuron and terminals. Right, an EM image showing a portion of a silver-intensified gold (SIG, white arrow) labeled neuron receiving inputs from GABAergic terminals (white asterisks) and other terminals (black asterisk). The green area covers the entire SIG-labeled neuron, the red arrowheads indicate the endings of GABAergic terminals aligned with the plasma membrane. The expressions for % GABA innervation and the density of GABAergic terminals are shown on the right. Scale bar = 500 nm. **b** Comparisons of % GABA innervation (left panel), and the GABA terminal density (right panel), between the mCherry + and mCherry-negative neurons. From the same DREADD experimental animal. **c** Comparisons and cumulative density funcions of the GABAergic terminal inter-synaptic lengths (right panel), and individual GABAergic terminal lengths (left panel) of the mCherry + ($n = 69$) and mCherry-negative ($n = 83$) neurons sampled across all of the DREADD experimental animals ($N = 7$). **d** Correlations between %mCherry + /cFos + and %GABA innervation (left panel), or GABAergic terminal density (right panel), of mCherry + and mCherry-negative neurons. Each point represents the averaged quantities from an individual DREADD experimental animal. Significant correlation is shown with straight line together with its p-value and r-square. *$p \leq 0.05$, **$p \leq 0.01$, ***$p \leq 0.001$

Correlations between the prevalence of mCherry + /cFos + dually immunofluorescent cells and GABAergic innervation

For the DREADD group, %mCherry + /cFos + (immunofluorescence data) was significantly and negatively correlated with %GABA innervation of mCherry + pyramidal cells (EM data) ($r^2 = 0.5912$, $p = 0.0434$) but not with the values of %GABA innervation of mCherry-negative neurons (Fig. 8d). This indicates that those individuals with relatively stronger GABAergic innervation of mPF→DR pyramidal neurons exhibited greater suppression of the mPFC→DR

pathway. In contrast, the correlation of the GABA terminal density with %mCherry+/cFos+ was not significant (Fig. 8d). This indicates that the percent coverage of the pyramidal neurons' cell bodies played a more significant role than the number of GABAergic terminals in modulating neuronal activity and that this GABAergic modulation was specific to the subpopulation of Layer 5 pyramidal neurons with projections to DR and driven by C21.

Correlation analysis of feeding behaviors during FR with immunofluorescence and EM data

To address whether the circuits involving the mPFC→DR were related to the feeding behaviors of mice undergoing ABA, correlation analyses of data obtained by EM (%GABA innervation of mCherry+ and mCherry-negative pyramidal cells), immunofluorescence (%mCherry+/cFos+, %GAD+/cFos+) and food intake of the DREADD group were performed. As shown in Fig. 9, food intake on FR days of ABA1 did not correlate with EM or immunofluorescence data.

During ABA2, %mCherry+/cFos+ correlated significantly and positively with food intake on FR2, the day when C21 was injected to activate the mPFC→DR pathway ($r^2 = 0.6091$, $p = 0.0384$) (Fig. 10a). These variables showed no correlation on FR1, FR3 or FR4 (Fig. 10a). The positive correlation conforms to the previous literature regarding DR's roles in feeding (Bendotti et al. 1986; Fletcher and Davies 1990; Nectow et al. 2017) as well as the connectivity between mPFC and DR (Jankowski and Sesack 2004).

While %GAD+/cFos+ appeared to be unrelated to feeding on FR2 (Fig. 10b), %GABA innervation only of mCherry+ (Fig. 10c) (i.e., not the mCherry-negative pyramidal neurons in Layer 5, Fig. 10d) exhibited a very significant negative correlation with the food intake specifically on FR2, when C21 was administered ($r^2 = 0.8429$, $p = 0.0035$).

Correlation analysis of wheel running during FR with immunofluorescence and EM data

In contrast to two correlations revealed for feeding behavior during FR, the only correlation revealed for wheel running during FR was with the extent of GABA innervation of the mCherry-negative Layer 5 pyramidal cells. The correlation was negative with the PP running on FR2 ABA2, when the mPFC-DR pathway was activated ($r^2 = 0.8639$, $p = 0.0024$). This negative correlation indicates that chemogenetic activation of the mPFC-DR recruited GABAergic interneurons in PFC, which may have enhanced the inhibition of the Layer 5 pyramidal neurons that project corticofugally to brain regions other than DR.

Discussion

This project combined chemogenetic stimulation with confocal and EM imaging to elucidate the connectivity of mPFC→DR pyramidal neurons and their roles in regulating feeding behaviors of mice in the ABA model. Contrary to our initial expectation, direct activation or inhibition of the mPFC→DR pathway by DREADDs did not yield an effect that could be detected as a group mean difference, relative to CON animals' behavior without chemogenetic modulation. Closer inspection revealed that this was due to the wide variance in behavior that obscured the neuromodulatory effects of DREADDs upon individuals. By pursuing correlative analysis of confocal data of individual animals, we revealed that individuals with greater DREADD-mediated activation of mPFC→DR pyramidal cells also exhibited greater food consumption (Fig. 10) and activation of GABA-INs (Fig. 6). Moreover, analysis of the EM data on GABAergic axo-somatic innervation, relative to food intake revealed a strong negative correlation: the more prevalent the GABAergic innervation of mPFC→DR pyramidal neurons, the more suppressed were an individual's food intake. Together, these findings reveal that mPFC does modulate feeding behavior within the context of ABA, with stronger GABAergic inhibition of the corticofugal pathway projecting to the DR resulting in reduced feeding.

The mPFC microcircuit activated by chemogenetic modulation of the mPFC→DR pyramidal neurons

Previous studies successfully modulated the mPFC→DR pathway through two approaches: Injecting currents into the DR-projecting pyramidal neurons in the mPFC (Celada et al. 2001), or optogenetically stimulating axons within DR with cell bodies of origin in the mPFC (Warden et al. 2012). The chemogenetic modulation of the mPFC→DR pathway was like the approach of Celada et al. (2001) in having a greater chance of recruiting other neurons within mPFC as well as other brain regions. Indeed, in our study, we showed that the direct chemogenetic activation of the DR-projecting pyramidal neurons in Layer 5 of mPFC also significantly boosted the activities of Layer 2/3 neurons, which were GABAergic and pyramidal (Fig. 5c). This means that microcircuits from DR-projecting Layer 5 pyramidal neurons feedback to Layers 2/3 of mPFC, in addition to the canonical cortical circuit with projections from Layers 2/3 pyramidal neurons to Layer 5 pyramidal neurons (Dhruv 2015).While this type of feedback pathway from deeper to superficial layers as well as their functional implications are well-studied in the visual cortex (reviewed in Capone et al. 2016), such circuits are less studied in the mPFC. At least some of the activated

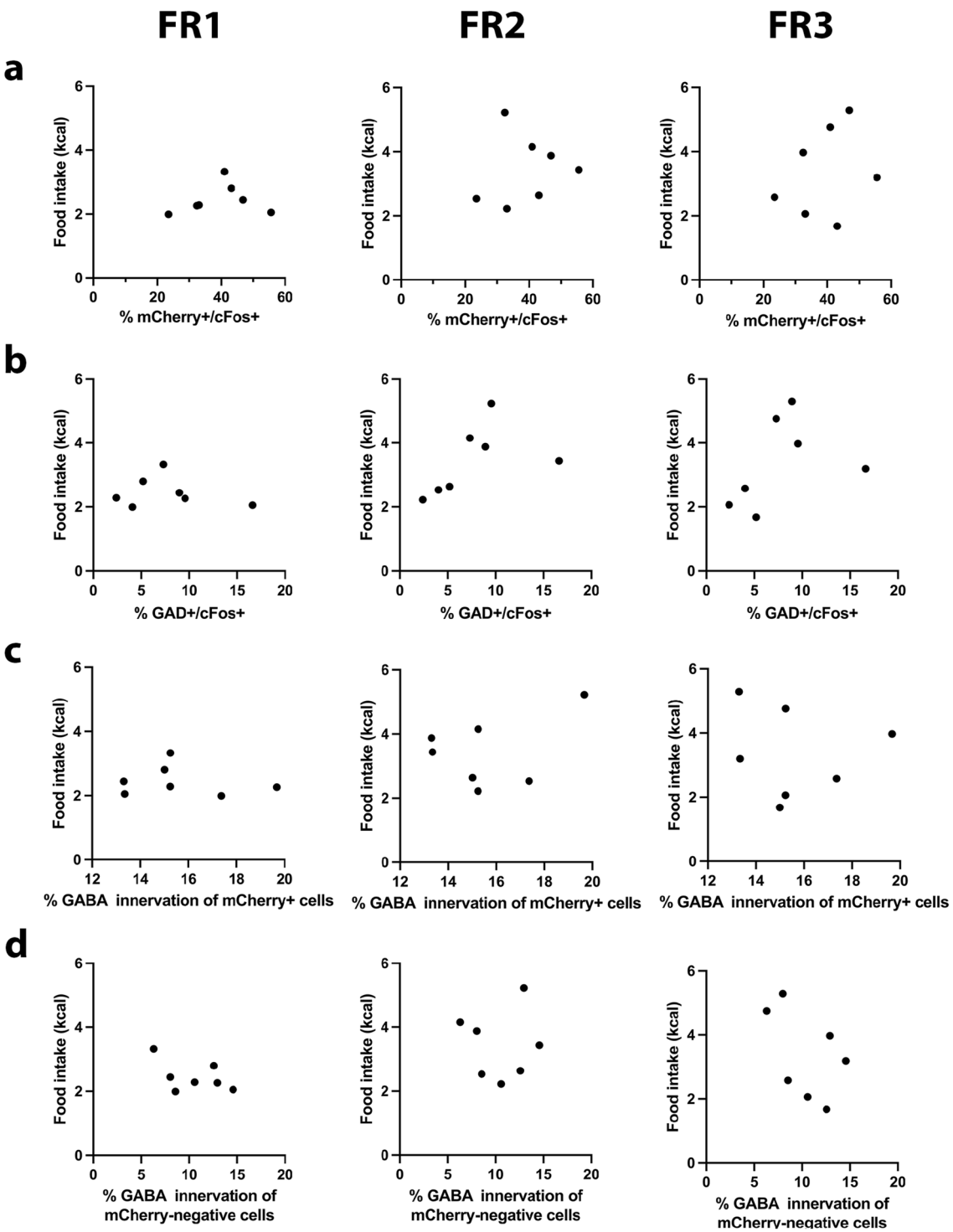

Fig. 9 Absence of correlations of feeding behaviors during ABA1 with the IF and EM data. Correlations between the food intake during the first ABA and %mCherry + cFos + (**a**), %GAD + cFos + (**b**), %GABA of mCherry + neurons (**c**) and %GABA of mCherry-negative neurons (**d**)

neurons in Layers 2/3 were pyramidal neurons which, in turn, are known to project to dorsal and ventral striatum (Jankowski and Sesack 2004) and enhance wheel running during FR within the context of ABA (Santiago et al. 2021). Those activities may exert complicated effects that were

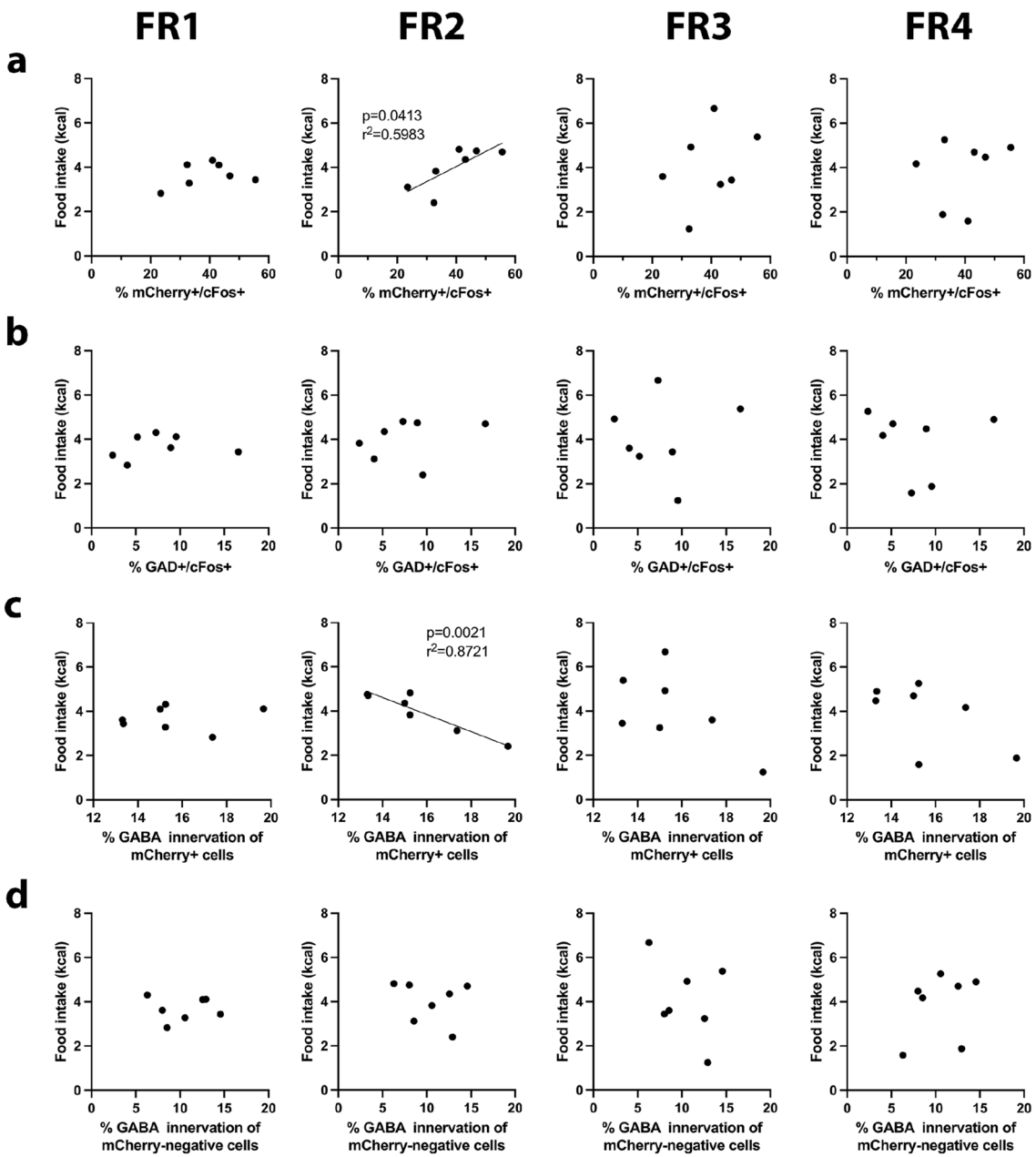

Fig. 10 Feeding behavior during FR2 of ABA2 correlates with IF and EM data. Correlations between the food intake during the second ABA and %mCherry+/cFos+(**a**), %GAD+/cFos+(**b**), %GABA innervation of mCherry+neurons (**c**) and %GABA innervation of mCherry-negative neurons (**d**). Significant correlations are indicated by straight lines together with their *p*-values and *r*-squares

intermingled with the roles of the DR-projecting neurons in regulating feeding of our ABA animals.

If the correlation between %GAD+/cFos+ and %mCherry+/cFos+ had been negative, this would have implied that firing of GABA-INs controlled excitability of mPFC→DR pyramidal cells. Instead, the correlation between these two variables was positive (Fig. 6c). This supports an alternative view—namely that firing of GABA-INs was driven by the mPFC→DR neurons. The idea that DR-projecting pyramidal neurons drive the GABA-INs across layers in mPFC conforms to the previous findings of local GABAergic microcircuits in mPFC (Sun et al. 2019). Activation of GABA-INs upon DREADD stimulation of the mPFC→DR pathway might be a way for the animals to avoid hyperactivity and excitotoxicity.

The current study showed that the overall activity of DR-projecting neurons could be affected significantly and negatively by the extent of GABAergic innervation that they

received (Fig. 8d). This illustrates a strong link between pyramidal neurons' firing and their ultrastructure—specifically, the axo-somatic synapses supporting negative feedback. Since greater firing (cFos immunoreactivity) of GABA-INs did not result in suppression of mPFC→DR pyramidal neurons, these findings, together, reveal that excitability of Layer 5 pyramidal neurons is dictated more by ultrastructure of axo-synaptic inputs formed by GABAergic axon terminals than by the firing properties of the GABA-IN.

A novel synaptic feature of mPFC→DR pyramidal neurons is revealed by EM-ICC: prevalent GABAergic innervation

The EM-immunocytochemical approach enabled us to distinguish the DR-projecting versus non-DR-projecting pyramidal neurons in Layer 5 of mPFC based on the immunoreactivity of pyramidal cell bodies to mCherry. Previous studies had shown that ABA could cause an enlargement in the GABAergic coverage of the Layer 5 pyramidal neurons in mPFC (Chen et al. 2016). The current study extends that finding by showing that the DR-projecting neurons receive more GABAergic innervation than other pyramidal neurons in Layer 5 of mPFC that do not project to DR (Fig. 8b). This could mean that the enlargement of GABAergic terminals in the mPFC of ABA animals specifically targets the DR-projecting subgroup. It is also likely that the DR-projecting neurons are more resistant to the chemogenetic stimulation due to the stronger inhibitory feedback that they receive.

Whether the greater GABAergic innervation is an intrinsic property of the DR-projecting neurons or reflects plastic change caused by the Gq-DREADD-induced hyperactivity remains to be investigated. We think the former is more likely. This thought is based on an earlier observation that Layer 5 pyramidal neurons of mPFC without projections to dorsal striatum (DS) exhibited greater GABAergic innervation than the corticostriatal neurons (CSt) labeled retrogradely from DS, even though these mPFC→DR pyramidal cells were not designed to be modulated by DREADD ligands (Santiago et al. 2021). This suggests that there are innate differences in GABAergic innervation across subpopulations of Layer 5 pyramidal neurons depending on their projection patterns. Although both the PT (pyramidal tract) and IT (intratelencephalic) subpopulations of Layer 5 neurons in motor and somatosensory cortex project to DS and are thus considered CSt (Reiner et al. 2003; Shepherd 2013), the extent of mPFC's PT collaterals to DS (which would include the mPFC→DR pyramidal cells studied here) is much less than for the mPFC's IT subpopulation of CSt pyramidal cells (Anastasiades and Carter 2021). Both our previous (Santiago et al. 2021) and current ultrastructural analyses indicate that the mPFC→DR/PT cells of Layer 5 belong to the subpopulation of neurons in Layer 5 of mPFC with greater GABAergic innervation. This agrees with electrophysiological studies indicating that the PT subpopulation of CSt in Layer 5 of mPFC are more strongly inhibited than are the IT-CSt neurons in Layer 5 (Anastasiades and Carter 2021; Lee et al. 2014).

Chemogenetic modulation of the mPFC→DR pathway enhances food intake

Although activation or inhibition of the mPFC-DR pathway by DREADDs did not significantly alter the group average of food intake of mice in the ABA model compared to control ABA animals lacking DREADD gene expression (Fig. 2d), correlation analysis performed for the experimental animals showed that individuals with greater activities among the DR-projecting pyramidal neurons exhibited greater food intake. Notably, the correlation between food intake and neuronal firing of mPFC→DR pyramidal neurons appeared only on FR2 of ABA2, and not FR1, 3 or 4 (Fig. 10a). Considering that C21 was injected only on FR2 to activate the mPFC→DR pathway, the following explanation is proposed: On FR2, activity of the mPFC→DR pathway may already have been very high due to animals' active coping with starvation stress (Amat et al. 2005). Under this circumstance, activation of the excitatory DREADDs by C21 may not have been able to boost the activity of the mPFC→DR pyramidal neurons any further. Instead, C21 could have generated differential activities of the DR-projecting pyramidal neurons (%mCherry+/cFos+) through differential GABAergic inhibition. On a related note, %GAD+/cFos+ did not correlate with food intake on any day of ABA2, even on FR2 when C21 was injected (Fig. 10b). This is probably because individual differences in the inhibitory effects caused by the activation of the GABA-INs in mPFC following C21 injection was not specific to the DR-projecting neurons, but acted on a wide range of neurons.

Individual differences in food intake is influenced by ultrastructural differences in GABAergic axo-somatic synapses on mPFC→DR pyramidal neurons more than by GABA neuronal firing

Importantly, the differential GABAergic inhibition appears to have resulted from differential levels in GABAergic neurons' axonal structure—i.e., the extent of axo-somatic innervation of mPFC→DR pyramidal neurons, rather than differential firing of GABA-INs. This idea is derived from the observation that correlation was evident between food intake and the extent of GABAergic innervation (%GABA,

EM data), specifically of pyramidal neurons with projections to DR (Fig. 10c) and not the pyramidal neurons lacking projections to DR (Fig. 10d), further supporting the idea that the mPFC→DR pathway is involved especially in the feeding behaviors of mice. The contrasting lack of correlation between the %GAD+/cFos+ and food intake is indication that the strength of GABAergic inhibition is influenced more by axonal structure than by the firing pattern of GABAergic neurons.

The correlation between %GABA innervation of mCherry+ pyramidal neurons and food intake is negative (Fig. 10c), while the correlation between mCherry+/cFos+ and food intake is positive (Fig. 10a). These two correlations with opposite valences agree with the notion that excitatory outflow from the mPFC to DR stimulates feeding and that synaptic plasticity underlying the gain of resilience to ABA (measured based on increased food intake) may be the *retraction* of GABAergic innervation of mPFC→DR pyramidal neurons.

Since activation of serotonergic neurons in the DR suppresses feeding (Nectow et al. 2017), the dominant targets of mPFC→DR in DR may be the GABA-IN that inhibit firing of the serotonergic neurons. Such direct pathway from pyramidal neurons in mPFC to GABA-IN in DR has been elucidated by EM (Jankowski and Sesack 2004), this may be an alternative or additional site of synaptic plasticity of animals that gain resilience following ABA induction. Further analysis of the activity of GABA-INs in the DR following chemogenetic activation of the mPFC→DR pyramidal neurons promises to yield data testing this hypothesis.

Two parallel pathways regulate feeding and running during ABA

Previous findings from our lab showed that the mPFC pyramidal neurons projecting to dorsal striatum (mPFC→DS) contribute to hyperactivity in the ABA model, but that this pathway did not alter food intake (Santiago et al. 2021). The current study complements those observations by identifying the mPFC→DR as a potential pathway regulating feeding in the ABA model. The current study reveals segregation of the behavioral effects linked to modulation of the DR-projecting and non-DR-projecting pyramidal neurons in Layer 5 of mPFC: (1) GABAergic innervation of mCherry+ neurons, but not of the mCherry-negative neurons, correlated significantly only with food intake but not with wheel running (Fig. 10); (2) GABAergic innervation of mCherry-negative neurons correlated negatively with PP running on FR2 of ABA2 when the mPFC→DR was activated, but exhibited little effect on feeding (Fig. 10). The bountiful distribution of mPFC→DS pyramidal neurons in Layer 5 of mPFC (Santiago et al. 2021) makes it likely that the mPFC→DS pyramidal neurons constitute a large portion of the mCherry-negative pyramidal neurons in the current study. If so, then the negative correlation between GABAergic innervation of mCherry-negative pyramidal neurons and PP running is in line with our previous findings that the chemogenetic inhibition of mPFC→DS neurons suppresses PP running (Santiago et al. 2021). We suggest two parallel pathways that may contribute to individual vulnerability to ABA: the mPFC→DR pathway that regulates feeding (current study), and the mPFC→DS pathway that controls food restriction-evoked hyperactivity (Santiago et al. 2021).

Lack of effect of SalB/KORD

If the ceiling effect was accountable for our observation of food intake on FR2, then SalB injection on FR4 should have significantly decreased the activity of the mPFC→DR pathway and thus decreased food intake of mice. However, this was not observed. A possible explanation for this is that further decrease in food intake on FR4 when the animals had already been food restricted for three days and had lost a significant amount of body weight would put them under severe danger of starving to death. Under this circumstance, other players such as the mPFC→lateral hypothalamus pathway which is also capable of regulating feeding (Petrovich et al. 2005) may have interfered with SalB modulation, thereby saving the animals from death.

Conclusion

We dissected the circuits in mPFC that involved the DR-projecting pyramidal neurons in Layer 5 through immunofluorescence and EM immunocytochemistry. Summarized in Fig. 11, we show that mPFC→DR pyramidal neurons send outputs not only to DR but also to Layer 2/3 pyramidal neurons and GABA-INs across layers. Thus, DREADD ligands modulate activity of a multi-synaptic mPFC circuitry rather than a single population of neurons. Through correlation analysis, we have gathered data supporting the hypothesis that mPFC→DR is a high-order regulator of feeding for ABA mice and possibly also for AN patients, favoring them to overcome the maladaptive behavior of FR, when activated. Conversely, the stronger the inhibition of this pathway, the more food restrictive individuals may become. This finding contrasts sharply from another recent finding from our lab, demonstrating that activation mPFC→DS exacerbates the food restriction-evoked wheel running of ABA mice (Santiago et al. 2021). On the question of whether the mPFC is the site for generating the decision to eat (i.e., adaptive for survival) or to run (i.e., maladaptive for mice in captivity), one factor influencing this decision may be the ratio of GABAergic innervations across the two parallel pathways. Within Layer 5 of ABA mice, the

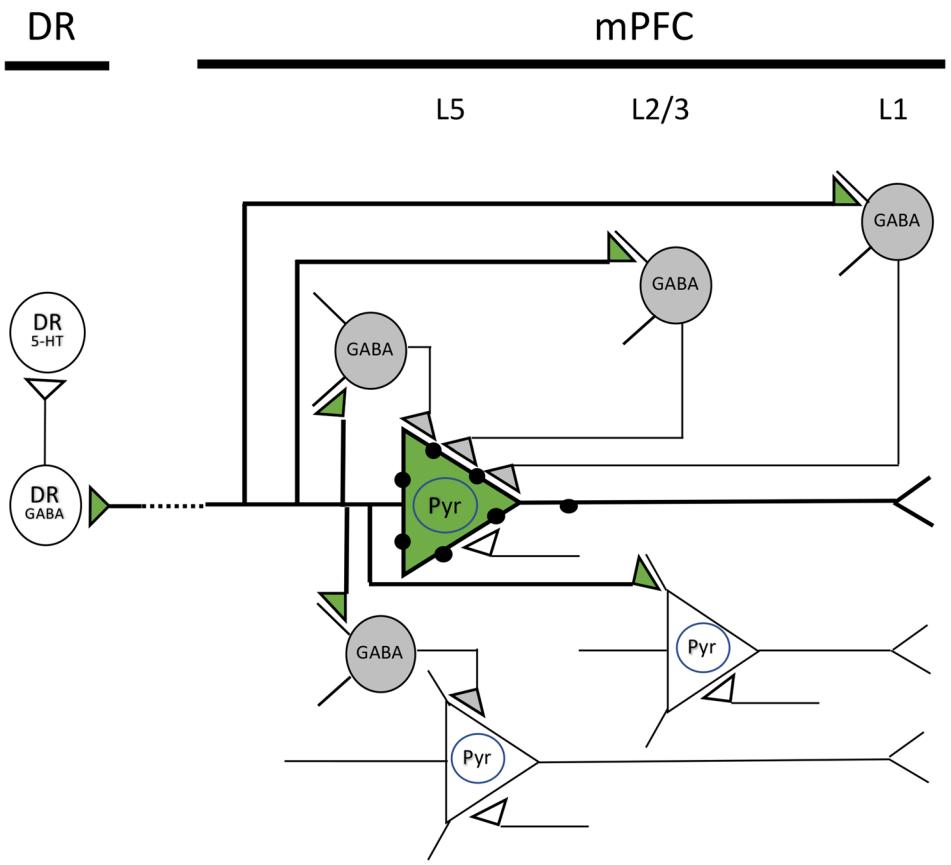

Fig. 11 Summary of the proposed microcircuit in mPFC that involves the DR-projecting pyramidal neurons. The DR-projecting neurons (green) are distinguished from the others because of the mCherry-tagged DREADDs on their membranes (black dots). While those neurons project to DR, they may also send outputs to Layer 2/3 pyramidal neurons and GABAergic neurons across layers in mPFC. Those DR-projecting neurons receive greater GABAergic innervation than other Layer 5 pyramidal neurons, which could make them more resistant to the chemogenetic excitation. Pyr, pyramidal neuron; G-IN, GABAergic interneuron; DRN^{GABA}, GABAergic neurons in DR; $DRN^{5\text{-}HT}$, serotonergic neuron in DR

mPFC→DR pyramidal neurons receive more GABAergic innervation than do the neurons projecting elsewhere, presumably including the mPFC→DS pyramidal neurons. This GABAergic innervation pattern may underlie individual differences in vulnerability to ABA, defined both as heightened wheel running (due to weaker inhibition of the mPFC→DS pathway) and stronger suppression of feeding (due to the stronger inhibition of the mPFC→DR pathway). For animals that have experienced ABA, the relative strength of GABAergic inhibition of the two corticofugal pathways originating in the mPFC may dictate ABA vulnerability, with those individuals showing more inhibition of the mPFC→DR pathway than of the mPFC→DS pathway being the more vulnerable. Although this study was set out to examine the role of corticofugal pyramidal neurons in an animal's decision to eat or run, data point to GABA-IN being the more influential cellular components in the formation of this decision. This idea is undergoing testing through chemogenetic modulation of GABA-IN in the mPFC.

Research on AN has uncovered the complexity of this mental illness at both the biological (Bulik et al. 2007) and the socio-cultural (Garner and Garfinkel 1980; Polivy and Herman 2002) levels. Though AN is not a purely monogenic mental illness such as Huntington's Disease, modern studies provide substantial evidence pointing to the genetic risk factors involved in it. For example, AN tends to aggregate in families (Holland et al. 1988; Strober et al. 2000), and an AN-susceptibility gene is proposed to be located on chromosome 1 (Grice et al. 2002). Besides, AN tends to affect females more than males (Smink et al. 2014; Timko et al. 2019), suggesting the involvement of sex steroids or chromosomes in the development of AN (Wable et al. 2015). The sex difference could also be due to greater socio-cultural stressors placed on female adolescents versus male (Collison and Barnier 2019; Garner and Garfinkel 1980; Polivy and Herman 2002; Thompson and Stice 2001). Furthermore, recent research could even trace the etiology of AN to an epigenetic level (Hubel et al. 2019). In addition to the biological risk factors, profound familial influences and socio-cultural factors such as the culture of abundance and peer influences also contribute to the cause of AN. The central role played by structural differences in GABAergic axonal arbors in generating individual differences in resilience/vulnerability to ABA highlight the importance of probing for genes linked to the GABAergic system and for designing pharmacological treatments that target GABA receptor activity for the treatment of AN.

Acknowledgements The authors thank the help of the following undergraduates in animal husbandry and daily data collection: Sabrina George, Ishan Handa, Emily Makowicz, Rose Temizer.

Author contributions All authors read and consented to the submitted manuscript. The original text was written by M. Du, then extensively revised by C Aoki and edited in its final stage by A. Santiago and C. Akiz. AS performed all of the surgeries. Daily Care of the animals was performed by AS and C. Aoki. All authors contributed to data analysis. AS and MD performed analysis of wheel running, body weight and food consumption. MD and C Akiz performed analysis of immunofluorescence data. MD and C Aoki performed analysis of EM data.

Funding The National Institutes of Health (EY13079; F31 MH112372; R25GM097634); the National Science Foundation (DBI-1460880); and New York University (NYU Research Challenge Fund; NYU Dean's Dissertation Fellowship); Vulnerable Brain Project.

Availability of data Raw data of wheel counts, body weight, food consumption, and images captured using the confocal and electron microscopes can be provided upon request.

Code availability Not applicable.

Declarations

Conflict of interest None of the authors have conflict of interest to disclose. None of the authors have relevant financial or non-financial interests to disclose.

Ethics approval All aspects of live animal handling followed the protocol approved by NYU's University Animal Welfare Committee and by the Institutional Animal Care and Use Committees of New York University (A3317-01).

Consent of publication All authors consent to the publication of the submitted manuscript.

References

Amat J, Baratta MV, Paul E, Bland ST, Watkins LR, Maier SF (2005) Medial prefrontal cortex determines how stressor controllability affects behavior and dorsal raphe nucleus. Nat Neurosci 8(3):365–371. https://doi.org/10.1038/nn1399

Anastasiades PG, Carter AG (2021) Circuit organization of the rodent medial prefrontal cortex. Trends Neurosci 44(7):550–563. https://doi.org/10.1016/j.tins.2021.03.006

Arcelus J, Mitchell AJ, Wales J, Nielsen S (2011) Mortality rates in patients with anorexia nervosa and other eating disorders. A meta-analysis of 36 studies. Arch Gen Psychiatry 68(7):724–731. https://doi.org/10.1001/archgenpsychiatry.2011.74

Attia E (2010) Anorexia nervosa: current status and future directions. Annu Rev Med 61:425–435. https://doi.org/10.1146/annurev.med.050208.200745

Ball K, Lee C (2000) Relationships between psychological stress, coping and disordered eating: a review. Psychol Health 14(6):1007–1035. https://doi.org/10.1080/08870440008407364

Bendotti C, Garattini S, Samanin R (1986) Hyperphagia caused by muscimol injection in the nucleus raphe dorsalis of rats: its control by 5-hydroxytryptamine in the nucleus accumbens. J Pharm Pharmacol 38(7):541–543. https://doi.org/10.1111/j.2042-7158.1986.tb04634.x

Birmingham CL, Su J, Hlynsky JA, Goldner EM, Gao M (2005) The mortality rate from anorexia nervosa. Int J Eat Disord 38(2):143–146

Bulik CM, Slof-Op't Landt MC, van Furth EF, Sullivan PF (2007) The genetics of anorexia nervosa. Annu Rev Nutr 27:263–275

Bullitt E (1990) Expression of c-fos-like protein as a marker for neuronal activity following noxious stimulation in the rat. J Comp Neurol 296(4):517–530. https://doi.org/10.1002/cne.902960402

Capone F, Paolucci M, Assenza F, Brunelli N, Ricci L, Fiorio L, Di Lazzaro V (2016) Canonical cortical circuits: current evidence and theoretical implications. Neurosci Neuroecon 5:1–8. https://doi.org/10.2147/NAN.S70816

Celada P, Puig MV, Casanovas JM, Guillazo G, Artigas F (2001) Control of dorsal raphe serotonergic neurons by the medial prefrontal cortex: Involvement of serotonin-1A, GABA(A), and glutamate receptors. J Neurosci 21(24):9917–9929

Chen X, Choo H, Huang XP, Yang X, Stone O, Roth BL, Jin J (2015) The first structure-activity relationship studies for designer receptors exclusively activated by designer drugs. ACS Chem Neurosci 6(3):476–484. https://doi.org/10.1021/cn500325v

Chen YW, Wable GS, Chowdhury TG, Aoki C (2016) Enlargement of axo-somatic contacts formed by GAD-immunoreactive axon terminals onto layer V pyramidal neurons in the medial prefrontal cortex of adolescent female mice is associated with suppression of food restriction-evoked hyperactivity and resilience to activity-based anorexia. Cereb Cortex 26(6):2574–2589. https://doi.org/10.1093/cercor/bhv087

Chowdhury TG, Wable GS, Sabaliauskas NA, Aoki C (2013) Adolescent female C57BL/6 mice with vulnerability to activity-based anorexia exhibit weak inhibitory input onto hippocampal CA1 pyramidal cells. Neuroscience 241:250–267. https://doi.org/10.1016/j.neuroscience.2013.03.020

Chowdhury TG, Wable GS, Chen YW, Tateyama K, Yu I, Wang JY et al (2019) Voluntary wheel running exercise evoked by food-restriction stress exacerbates weight loss of adolescent female rats but also promotes resilience by enhancing GABAergic inhibition of pyramidal neurons in the dorsal Hippocampus. Cereb Cortex 29(10):4035–4049. https://doi.org/10.1093/cercor/bhy283

Collison J, Barnier E (2019) Eating disorders, body dysmorphic disorder, and body image pathology in female Australian models. Clin Psychol 24:155–165. https://doi.org/10.1111/cp.12208

Compan V, Walsh BT, Kaye W, Geliebter A (2015) How does the brain implement adaptive decision making to eat? J Neurosci 35(41):13868–13878. https://doi.org/10.1523/JNEUROSCI.2602-15.2015

Connan F, Campbell IC, Katzman M, Lightman SL, Treasure J (2003) A neurodevelopmental model for anorexia nervosa. Physiol Behav 79(1):13–24. https://doi.org/10.1016/s0031-9384(03)00101-x

Correia PA, Matias S, Mainen ZF (2017) Stereotaxic adeno-associated virus injection and cannula implantation in the dorsal raphe nucleus of mice. Bio Protoc 7(18):e2549. https://doi.org/10.21769/BioProtoc.2549

Dahl RE (2004) Adolescent brain development: a period of vulnerabilities and opportunities. Keynote address. Ann N Y Acad Sci 1021:1–22. https://doi.org/10.1196/annals.1308.001

Dhruv NT (2015) Rethinking canonical cortical circuits. Nat Neurosci 18(11):1538. https://doi.org/10.1038/nn1115-1538

Fletcher PJ, Davies M (1990) Dorsal raphe microinjection of 5-HT and indirect 5-HT agonists induces feeding in rats. Eur J Pharmacol 184(2–3):265–271. https://doi.org/10.1016/0014-2999(90)90618-g

Foldi CJ, Milton LK, Oldfield BJ (2017) The role of mesolimbic reward neurocircuitry in prevention and rescue of the activity-based

anorexia (ABA) phenotype in rats. Neuropsychopharmacology 42(12):2292–2300. https://doi.org/10.1038/npp.2017.63
Fuhrmann D, Knoll LJ, Blakemore SJ (2015) Adolescence as a sensitive period of brain development. Trends Cogn Sci 19(10):558–566. https://doi.org/10.1016/j.tics.2015.07.008
Garner DM, Garfinkel PE (1980) Socio-cultural factors in the development of anorexia nervosa. Psychol Med 10(4):647–656. https://doi.org/10.1017/s0033291700054945
Giedd JN, Blumenthal J, Jeffries NO, Castellanos FX, Liu H, Zijdenbos A et al (1999) Brain development during childhood and adolescence: a longitudinal MRI study. Nat Neurosci 2(10):861–863. https://doi.org/10.1038/13158
Global Burden of Disease Study 2013 Collaborators (2013) Global, regional, and national incidence, prevalence, and years lived with disability for 301 acute and chronic diseases and injuries in 188 countries, 1990–2013: a systematic analysis for the Global Burden of Disease Study 2013. The Lancet 386(9995):743–800. https://doi.org/10.1016/S0140-6736(15)60692-4
Grahn RE, Will MJ, Hammack SE, Maswood S, McQueen MB, Watkins LR, Maier SF (1999) Activation of serotonin-immunoreactive cells in the dorsal raphe nucleus in rats exposed to an uncontrollable stressor. Brain Res 826(1):35–43. https://doi.org/10.1016/s0006-8993(99)01208-1
Grice DE, Halmi KA, Fichter MM, Strober M, Woodside DB, Treasure JT et al (2002) Evidence for a susceptibility gene for anorexia nervosa on chromosome 1. Am J Hum Genet 70(3):787–792. https://doi.org/10.1086/339250
Hall JF, Smith K, Schnitzer SB, Hanford PV (1953) Elevation of activity level in the rat following transition from ad libitum to restricted feeding. J Comp Physiol Psychol 46(6):429–433
Han W, Tellez LA, Perkins MH, Perez IO, Qu T, Ferreira J et al (2018) A neural circuit for gut-induced reward. Cell 175(3):887–888. https://doi.org/10.1016/j.cell.2018.10.018
Hardaway JA, Crowley NA, Bulik CM, Kash TL (2015) Integrated circuits and molecular components for stress and feeding: implications for eating disorders. Genes Brain Behav 14(1):85–97. https://doi.org/10.1111/gbb.12185
Holland AJ, Sicotte N, Treasure J (1988) Anorexia nervosa: evidence for a genetic basis. J Psychosom Res 32(6):561–571. https://doi.org/10.1016/0022-3999(88)90004-9
Hubel C, Marzi SJ, Breen G, Bulik CM (2019) Epigenetics in eating disorders: a systematic review. Mol Psychiatry 24(6):901–915. https://doi.org/10.1038/s41380-018-0254-7
Hudson JI, Hiripi E, Pope HG Jr, Kessler RC (2007) The prevalence and correlates of eating disorders in the National Comorbidity Survey Replication. Biol Psychiatry 61(3):348–358. https://doi.org/10.1016/j.biopsych.2006.03.040
Jankowski MP, Sesack SR (2004) Prefrontal cortical projections to the rat dorsal raphe nucleus: ultrastructural features and associations with serotonin and gamma-aminobutyric acid neurons. J Comp Neurol 468(4):518–529. https://doi.org/10.1002/cne.10976
Jean A, Laurent L, Delaunay S, Doly S, Dusticier N, Linden D et al (2017) Adaptive control of dorsal raphe by 5-HT4 in the prefrontal cortex prevents persistent hypophagia following stress. Cell Rep 21(4):901–909. https://doi.org/10.1016/j.celrep.2017.10.003
Kaye WH, Fudge JL, Paulus M (2009) New insights into symptoms and neurocircuit function of anorexia nervosa. Nat Rev Neurosci 10(8):573–584. https://doi.org/10.1038/nrn2682
Lee AT, Gee SM, Vogt D, Patel T, Rubenstein JL, Sohal VS (2014) Pyramidal neurons in prefrontal cortex receive subtype-specific forms of excitation and inhibition. Neuron 81(1):61–68. https://doi.org/10.1016/j.neuron.2013.10.031
Marti O, Marti J, Armario A (1994) Effects of chronic stress on food intake in rats: influence of stressor intensity and duration of daily exposure. Physiol Behav 55(4):747–753. https://doi.org/10.1016/0031-9384(94)90055-8
Merikangas KR, He JP, Burstein M, Swanson SA, Avenevoli S, Cui L et al (2010) Lifetime prevalence of mental disorders in U.S. adolescents: results from the National Comorbidity Survey Replication-Adolescent Supplement (NCS-A). J Am Acad Child Adolesc Psychiatry 49(10):980–989. https://doi.org/10.1016/j.jaac.2010.05.017
Nectow AR, Schneeberger M, Zhang H, Field BC, Renier N, Azevedo E et al (2017) Identification of a brainstem circuit controlling feeding. Cell 170(3):429–442. https://doi.org/10.1016/j.cell.2017.06.045
Nichols IS, Jones MI, Okere C, Ananaba G, Bush B, Gray C et al (2017) Nitrergic neurons of the dorsal raphe nucleus encode information about stress duration. PLoS ONE 12(11):e0187071. https://doi.org/10.1371/journal.pone.0187071
Nishitani N, Nagayasu K, Asaoka N, Yamashiro M, Andoh C, Nagai Y et al (2019) Manipulation of dorsal raphe serotonergic neurons modulates active coping to inescapable stress and anxiety-related behaviors in mice and rats. Neuropsychopharmacology 44(4):721–732. https://doi.org/10.1038/s41386-018-0254-y
Petrovich GD, Holland PC, Gallagher M (2005) Amygdalar and prefrontal pathways to the lateral hypothalamus are activated by a learned cue that stimulates eating. J Neurosci 25(36):8295–8302. https://doi.org/10.1523/JNEUROSCI.2480-05.2005
Polivy J, Herman CP (2002) Causes of eating disorders. Annu Rev Psychol 53:187–213. https://doi.org/10.1146/annurev.psych.53.100901.135103
Pollano A, Trujillo V, Suarez MM (2018) How does early maternal separation and chronic stress in adult rats affect the immunoreactivity of serotonergic neurons within the dorsal raphe nucleus? Stress 21(1):59–68. https://doi.org/10.1080/10253890.2017.1401062
Reiner A, Jiao Y, Del Mar N, Laverghetta AV, Lei WL (2003) Differential morphology of pyramidal tract-type and intratelencephalically projecting-type corticostriatal neurons and their intrastriatal terminals in rats. J Comp Neurol 457(4):420–440. https://doi.org/10.1002/cne.10541
Roux P, Blanchard JM, Fernandez A, Lamb N, Jeanteur P, Piechaczyk M (1990) Nuclear localization of c-Fos, but not v-Fos proteins, is controlled by extracellular signals. Cell 63(2):341–351. https://doi.org/10.1016/0092-8674(90)90167-d
Santiago AN, Makowicz EA, Du M, Aoki C (2021) Food restriction engages prefrontal corticostriatal cells and local microcircuitry to drive the decision to run versus conserve energy. Cereb Cortex 31(6):2868–2885. https://doi.org/10.1093/cercor/bhaa394
Shepherd GM (2013) Corticostriatal connectivity and its role in disease. Nat Rev Neurosci 14(4):278–291. https://doi.org/10.1038/nrn3469
Smink FR, van Hoeken D, Oldehinkel AJ, Hoek HW (2014) Prevalence and severity of DSM-5 eating disorders in a community cohort of adolescents. Int J Eat Disord 47(6):610–619. https://doi.org/10.1002/eat.22316
Strober M, Freeman R, Lampert C, Diamond J, Kaye W (2000) Controlled family study of anorexia nervosa and bulimia nervosa: evidence of shared liability and transmission of partial syndromes. Am J Psychiatry 157(3):393–401. https://doi.org/10.1176/appi.ajp.157.3.393
Sun Q, Li X, Ren M, Zhao M, Zhong Q, Ren Y et al (2019) A whole-brain map of long-range inputs to GABAergic interneurons in the mouse medial prefrontal cortex. Nat Neurosci 22(8):1357–1370. https://doi.org/10.1038/s41593-019-0429-9
Takase LF, Nogueira MI (2008) Patterns of fos activation in rat raphe nuclei during feeding behavior. Brain Res 1200:10–18. https://doi.org/10.1016/j.brainres.2008.01.036
Tervo DG, Hwang BY, Viswanathan S, Gaj T, Lavzin M, Ritola KD et al (2016) A designer AAV variant permits efficient retrograde

access to projection neurons. Neuron 92(2):372–382. https://doi.org/10.1016/j.neuron.2016.09.021
Thompson JK, Stice R (2001) Thin-ideal internalization: mounting evidence for a new risk factor for body-image disturbance and eatng pathology. Curr Dir Psychol Sci 10(5):181–183
Thompson KJ, Khajehali L, Bradley SJ, Navarrete JS, Huang XP, Slocum S et al (2018) DREADD agonist 21 is an effective agonist for muscarinic-based DREADDs in vitro and in vivo. ACS Pharmacol Transl Sci 1(1):61–72. https://doi.org/10.1021/acsptsci.8b00012
Timko CA, DeFilipp L, Dakanalis A (2019) Sex differences in adolescent anorexia and bulimia nervosa: beyond the signs and symptoms. Curr Psychiatry Rep 21(1):1. https://doi.org/10.1007/s11920-019-0988-1
Tomioka R, Sakimura K, Yanagawa Y (2015) Corticofugal GABAergic projection neurons in the mouse frontal cortex. Front Neuroanat 9:133. https://doi.org/10.3389/fnana.2015.00133
Vardy E, Robinson JE, Li C, Olsen RHJ, DiBerto JF, Giguere PM et al (2015) A new DREADD facilitates the multiplexed chemogenetic interrogation of behavior. Neuron 86(4):936–946. https://doi.org/10.1016/j.neuron.2015.03.065
Wable GS, Chen YW, Rashid S, Aoki C (2015) Exogenous progesterone exacerbates running response of adolescent female mice to repeated food restriction stress by changing alpha4-GABAA receptor activity of hippocampal pyramidal cells. Neuroscience 310:322–341. https://doi.org/10.1016/j.neuroscience.2015.09.006
Warden MR, Selimbeyoglu A, Mirzabekov JJ, Lo M, Thompson KR, Kim SY et al (2012) A prefrontal cortex-brainstem neuronal projection that controls response to behavioural challenge. Nature 492(7429):428–432. https://doi.org/10.1038/nature11617
Weissbourd B, Ren J, DeLoach KE, Guenthner CJ, Miyamichi K, Luo L (2014) Presynaptic partners of dorsal raphe serotonergic and GABAergic neurons. Neuron 83(3):645–662. https://doi.org/10.1016/j.neuron.2014.06.024
White EL (1989) Cortical circuits: synaptic organization of the cerebral cortex - structure, function, and theory. Birkhouser, Boston
Wouterlood FG, Jorritsma-Byham B (1993) The anterograde neuroanatomical tracer biotinylated dextran-amine: comparison with the tracer Phaseolus vulgaris-leucoagglutinin in preparations for electron microscopy. J Neurosci Methods 48(1–2):75–87. https://doi.org/10.1016/s0165-0270(05)80009-3